JACC Vol. 40, No. 5, 2002
September 4, 2002:998–1005

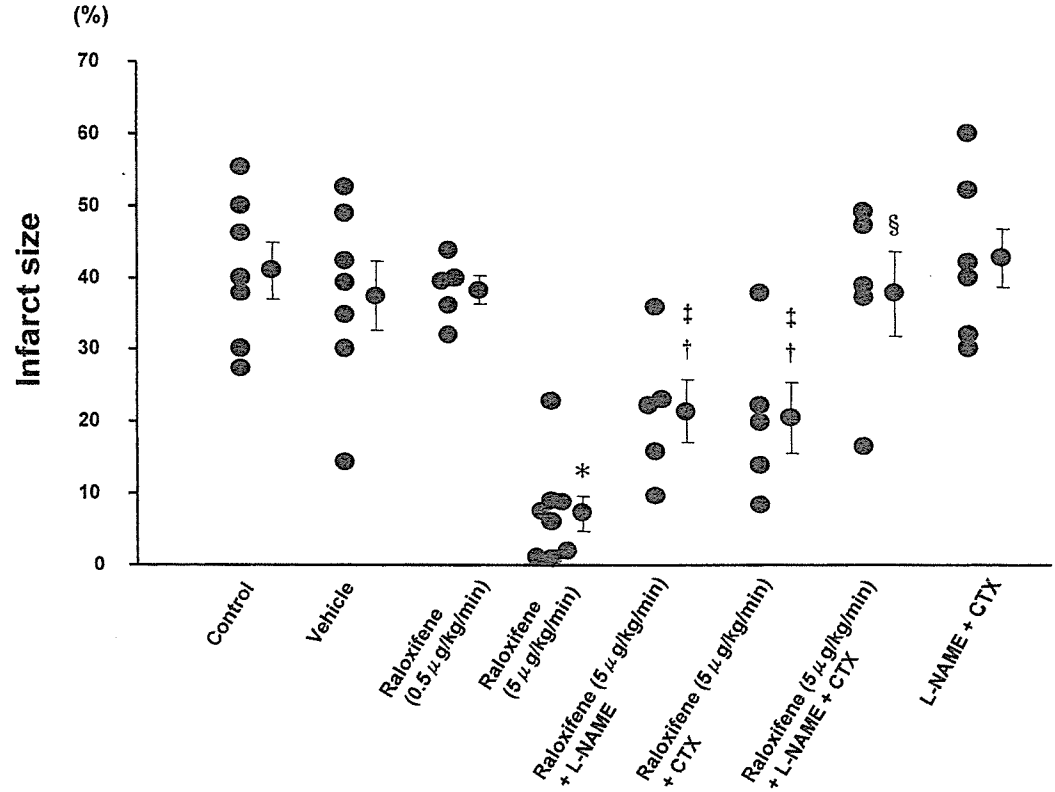

Figure 2. Infarct size as a percentage of the area at risk in the various experimental groups. Data from individual animals and mean ± SE values are shown. *p < 0.01 vs. control group. †p < 0.05 vs. raloxifene (5 μg/kg per min) group. ‡p < 0.05 vs. control group. §p < 0.01 vs. raloxifene (5 μg/kg per min) group. CTX = charybdotoxin; L-NAME = N^G-nitro-L-arginine methyl ester.

ischemic state was abolished by co-administration of L-NAME and CTX with raloxifene.

Myocardial MPO activity. Data on MPO activity for the ischemic and nonischemic regions of all experimental groups are shown in Table 4. These results showed that MPO activity significantly decreased only in the raloxifene (5 μg/kg per min) group, compared with the control group, suggesting that raloxifene reduced myocardial ischemia-reperfusion injury by attenuation of MPO activity.

Table 3. Percentage of Survival and Incidence of Ventricular Fibrillation in Each Group

Group	Survival (n/N)	Incidence of VF
Control	88.9% (8/9)	44.4%
Vehicle	100% (9/9)	33.3%
Raloxifene (0.5 μg/kg per min)	100% (6/6)	33.3%
Raloxifene (5 μg/kg per min)	100% (9/9)	11.1%*
Raloxifene (5 μg/kg per min) + L-NAME	71.4% (5/7)	42.9%
Raloxifene (5 μg/kg per min) + CTX	100% (7/7)	28.6%
Raloxifene (5 μg/kg per min) + L-NAME + CTX	85.7% (6/7)	42.9%
L-NAME + CTX	87.5% (7/8)	37.5%

*p < 0.05 vs. control group.
Abbreviations as in Table 1.

DISCUSSION

We have shown that raloxifene reduces the MI size and the incidence of ischemia- and reperfusion-induced VF in dogs and that these cardioprotective effects are blocked by either inhibition of NO synthase or antagonism of K_{Ca} channels. Moreover, only treatment with L-NAME and CTX does not exacerbate the infarct size and incidence of VF, compared with the control group. These results suggest that augmentation of endogenous NO release and opening of K_{Ca} channels induced by raloxifene synergistically contribute to the alleviation of irreversible ischemia-reperfusion injury. Furthermore, p38 MAP kinase activity in myocardial ischemia was reduced by raloxifene, suggesting that inhibition of p38 MAP kinase–signaling pathways is cardioprotective, as previously described (13,14), and this may partly explain the effects of raloxifene on ischemia-reperfusion injury.

Mechanisms of cardioprotective effects against ischemia- and reperfusion-induced injury mediated by NO and opening of K_{Ca} channels. The present results demonstrate that raloxifene attenuated infarct size and incidence of VF during reperfusion by cardioprotective mechanisms mediated by both NO and the opening of K_{Ca} channels. Potentiation of NO release may be an effective pharmacologic intervention to limit MI size, given that the administration of an NO donor markedly attenuates ischemia-

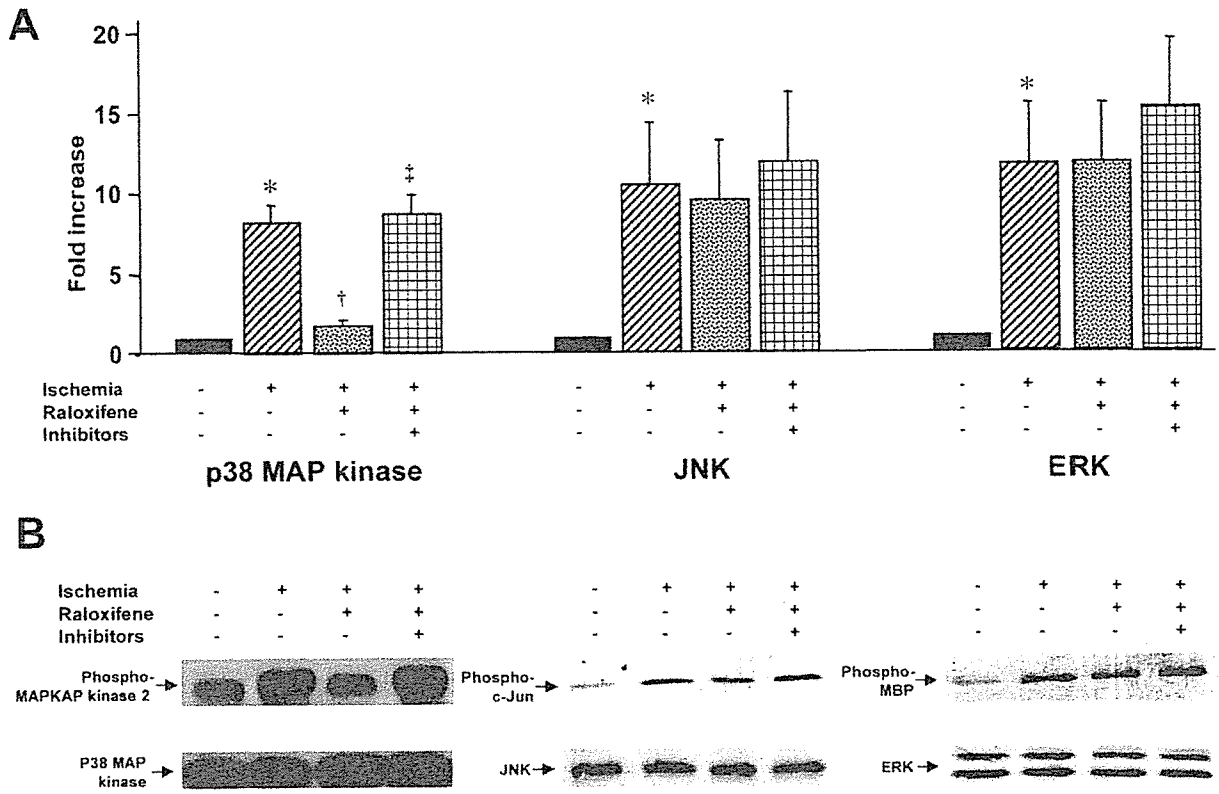

Figure 3. **(A)** Increases in p38 MAP kinase, JNK, and ERK activities in each group, compared with the "no ischemia" group, are shown (mean ± SE, n = 3 in each group). These MAP kinases were all activated during ischemia, whereas only p38 MAP kinase was inhibited by infusion of raloxifene into the coronary artery. The activities of the three kinases have been normalized to their total content. *$p < 0.01$ vs. group with no ischemia. †$p < 0.05$ vs. group with ischemia. ‡$p < 0.05$ vs. group with raloxifene pretreatment without inhibitors (e.g., L-NAME and CTX). **(B)** Representative results in each kinase are shown.

reperfusion injury (21,22). Several possible mechanisms may underlie the beneficial effects of NO on infarct size. First, because NO regulates the membrane Ca^{2+} current of cardiac cells (23), it may reduce the severity of ischemia by inhibiting the cytosolic accumulation of Ca^{2+}. Second, NO may also reduce oxygen-derived free radical generation by decreasing lipolysis, thereby limiting the generation of radicals through lipid peroxidation (24). It is not clear how raloxifene increases the release of NO in the reperfused heart, but a previous report demonstrated that raloxifene caused an immediate and marked production and release of NO in human endothelial cells (25). Increases in the cardiac NO level can also provoke protective effects against VF during reperfusion.

Table 4. Myeloperoxidase Activity of the Reperfused Myocardium

	Ischemic Area (U/g protein)	Nonischemic Area (U/g protein)
Control	20.1 ± 3.1	4.6 ± 1.1
Vehicle	19.9 ± 5.1	3.8 ± 1.3
Raloxifene (0.5 μg/kg per min)	22.9 ± 4.9	4.4 ± 1.2
Raloxifene (5 μg/kg per min)	6.6 ± 1.9*	4.7 ± 1.2
Raloxifene (5 μg/kg per min) + L-NAME	14.4 ± 2.9	5.5 ± 2.2
Raloxifene (5 μg/kg per min) + CTX	11.5 ± 2.3	4.8 ± 2.5
Raloxifene (5 μg/kg per min) + L-NAME + CTX	25.9 ± 2.8	3.1 ± 0.8
L-NAME + CTX	22.1 ± 2.5	3.7 ± 0.7

*$p < 0.05$ vs. control group. Data are presented as the mean value ± SE. Abbreviations as in Table 1.

Opening of K_{Ca} channels may hyperpolarize the cellular membrane and reduce Ca^{2+} overload during ischemia and reperfusion, similar to the protective effect of ATP-sensitive K^+ channels (26), in addition to its coronary vasodilatory effect (17). The precise mechanism by which the opening of K_{Ca} channels reduces VF during reperfusion is unknown. Although opening of K_{Ca} channels may reduce the duration of action potentials during coronary occlusion, resulting in an arrhythmogenic effect, this opening reduces Ca^{2+} overload in cardiomyocytes as a result of a hyperpolarized membrane potential.

Role of p38 MAP kinases in infarct size–limiting and anti-arrhythmic effects. We have shown that three major MAP kinases, including p38 MAP kinase, JNK, and ERK, were activated by ischemia and that raloxifene reduced only p38 MAP kinase activity, but not JNK and ERK, in canine hearts. Activation of p38 MAP kinase, JNK, and ERK in cardiomyocytes subjected to ischemia was previously reported (15,16), but the present study is the first to demonstrate an increase of MAP kinase activity in ischemic canine

hearts in vivo. Activation of ERK may be part of a "survival pathway," whereas activation of p38 MAP kinase and JNK represents a "death pathway" in the heart (27). In our study, increased activity of ERK was equal to that of JNK and less than that of p38 MAP kinase (Fig. 3). It is possible that the beneficial effects of ERK against ischemia might be abrogated by activation of both p38 MAP kinase and JNK in the ischemic heart. Some reports demonstrated that inhibition of p38 MAP kinase was effective for cardioprotection (13,14,28). In our study, p38 MAP kinase activation was attenuated by raloxifene during ischemia, and it may be reasonable that raloxifene has MI size–limiting and anti-arrhythmic effects by inhibition of the p38 MAP kinase–signaling pathway.

p38 MAP kinase regulates transcription factors, which respond to transcriptional changes in nuclei. In this study, there was a rapid and pronounced effect of raloxifene against ischemia-reperfusion injury, suggesting that raloxifene develops its effect by non-genomic means. p38 MAP kinase mediates myocardial ischemia-reperfusion–induced cytokines and free radical production (29,30), neutrophil activation (31), and platelet aggregation (32). It is possible to explain that the infarct size–limiting and anti-arrhythmic effects induced by raloxifene in our early-phase experiments are partly due to a reduction of ischemia-induced neutrophil activation accompanied by p38 MAP kinase inhibition, because the increased myocardial MPO activity of the ischemic area was actually diminished to the level of the nonischemic area by raloxifene infusion (5 μg/kg per min) (Table 4). Although the relationship between p38 MAP kinase, K_{Ca} channels, and NO is unclear, co-administration of L-NAME and CTX with raloxifene abolished the attenuation of p38 MAP kinase activity by treatment with raloxifene in our present study (Fig. 3), suggesting that p38 MAP kinase activity may be inhibited by NO and opening of K_{Ca} channels under ischemic stress. In contrast, we could not deny the possible mechanism that inhibition of p38 MAP kinase activity by raloxifene in ischemia may result in both an increased NO level and opening of K_{Ca} channels, because inhibition of p38 MAP kinase activity reduces the production of free radicals during ischemia and reperfusion, subsequently increasing the impaired NO synthase activity (29). Nitric oxide, opening of K_{Ca} channels, and inhibition of p38 MAP kinase possibly contribute to the mechanisms of cardioprotection against ischemia and reperfusion.

Clinical implications. To the best of our knowledge, this is the first report to demonstrate the MI size–limiting and anti-arrhythmic effects of raloxifene. In another report (33), idoxifene, one of the selective estrogen modulators, like raloxifene, had a beneficial effect on vascular remodeling in the balloon denudation rat model. Together with this action, raloxifene could be a good therapeutic drug for ischemic heart diseases. Moreover, raloxifene would be expected to be more advantageous and selective for the cardiovascular system, compared with estrogen, and it is possible to use raloxifene not only in postmenopausal women but also in premenopausal women with coronary heart diseases.

Acknowledgments

We thank Hideki Koyama, Akiko Ogai, Tomi Fukushima, and Junko Yamada for their technical assistance and advice.

Reprint requests and correspondence: Dr. Koichi Node, Department of Internal Medicine and Therapeutics, Osaka University Graduate School of Medicine, 2-2 Yamada-oka, Suita, 565-0871, Osaka, Japan. E-mail: node@medone.med.osaka-u.ac.jp.

REFERENCES

1. Stampfer MJ, Colditz GA, Wilett WC, et al. Postmenopausal estrogen therapy and cardiovascular disease: ten-year results from the Nurses' Health Study. N Engl J Med 1991;325:756–62.
2. Node K, Kitakaze M, Kosaka H, Minamino T, Funaya H, Hori M. Amelioration of ischemia- and reperfusion-induced myocardial injury by 17β-estradiol: role of nitric oxide and calcium-activated potassium channels. Circulation 1997;96:1953–63.
3. Node K, Kitakaze M, Kosaka H, et al. Roles of NO and Ca^{2+}-activated K^+ channels in coronary vasodilation induced by 17β-estradiol in ischemic heart failure. FASEB J 1997;11:793–9.
4. Boyle P, Maisonneuve P, Autier P. Update on cancer control in women. Int J Gynaecol Obstet 2000;70:263–303.
5. Douketis JD, Gordon M, Johnston M, Julian JA, Adachi JR, Ginsberg JS. The effects of hormone replacement therapy on thrombin generation, fibrinolysis inhibition, and resistance to activated protein C: prospective cohort study and review of the literature. Thromb Res 2000;99:25–34.
6. Delmas PD, Bjarnason NH, Mitlak BH, et al. Effects of raloxifene on bone mineral density, serum cholesterol concentrations, and uterine endometrium in postmenopausal women. N Engl J Med 1997;337:1641–7.
7. Draper MW, Flowers DE, Huster WJ, Neild JA, Harper KD, Arnaud C. A controlled trial of raloxifene (LY139481) HCl: impact on bone turnover and serum lipid profile in healthy postmenopausal women. J Bone Miner Res 1996;11:835–42.
8. Heaney RP, Draper MW. Raloxifene and estrogen: comparative bone-remodeling kinetics. J Clin Endocrinol Metab 1997;82:3245–9.
9. Walsh BW, Kuller LH, Wild RA, et al. Effects of raloxifene on serum lipids and coagulation factors in healthy post-menopausal women. JAMA 1998;279:1445–51.
10. Ettinger B, Black DM, Mitlak BH, et al, the Multiple Outcomes of Raloxifene Evaluation (MORE) Investigators. Reduction of vertebral fracture risk in postmenopausal women with osteoporosis treated with raloxifene: results from a 3-year randomized clinical trial. JAMA 1999;282:637–45.
11. Figtree GA, Lu Y, Webb CM, Collins P. Raloxifene acutely relaxes rabbit coronary arteries in vitro by an estrogen receptor–dependent and nitric oxide–dependent mechanism. Circulation 1999;100:1095–101.
12. Robinson MJ, Cobb MH. Mitogen-activated protein kinase pathways. Curr Opin Cell Biol 1997;9:180–6.
13. Ma XL, Kumar S, Gao F, et al. Inhibition of p38 mitogen-activated protein kinase decreases cardiomyocyte apoptosis and improves cardiac function after myocardial ischemia and reperfusion. Circulation 1999;99:1685–91.
14. Mackay K, Mochly-Rosen D. An inhibitor of p38 mitogen-activated protein kinase protects neonatal cardiac myocytes from ischemia. J Biol Chem 1999;274:6272–9.
15. Knight RJ, Buxton DB. Stimulation of *c*-Jun kinase and mitogen-activated protein kinase by ischemia and reperfusion in the perfused rat heart. Biochem Biophys Res Commun 1996;218:83–8.
16. Yue TL, Wang C, Gu JL, et al. Inhibition of extracellular signal–regulated kinase enhances ischemia/reoxygenation-induced apoptosis in cultured cardiac myocytes and exaggerates reperfusion injury in isolated perfused heart. Circ Res 2000;86:692–9.

17. Node K, Kitakaze M, Kosaka H, et al. Plasma nitric oxide end products are increased in the ischemic canine heart. Biochem Biophys Res Commun 1995;211:370–4.
18. Node K, Kitakaze M, Kosaka H, Minamino T, Hori M. Bradykinin mediation of Ca^{2+}-activated K^{+} channels regulates coronary blood flow in ischemic myocardium. Circulation 1997;95:1560–7.
19. Mori H, Haruyama S, Shinozaki Y, et al. New nonradioactive microspheres and more sensitive x-ray fluorescence to measure regional blood flow. Am J Physiol 1992;263:H1946–57.
20. Asanuma H, Kitakaze M, Funaya H, et al. Nifedipine limits infarct size via NO-dependent mechanisms in dogs. Basic Res Cardiol 2001;96:497–505.
21. Ma XL, Weyrich AS, Lefer DJ, Lefer AM. Diminished basal nitric oxide release after myocardial ischemia and reperfusion promotes neutrophil adherence to coronary endothelium. Circ Res 1993;72:403–12.
22. Lefer DJ, Nakanishi K, Johnston WE, Vinten-Johansen J. Antineutrophil and myocardial protecting action of a novel nitric oxide donor after acute myocardial ischemia and reperfusion in dogs. Circulation 1993;88:2337–50.
23. Mery PF, Pavoine C Belhassen, Pecker F, Fishmeister R. Nitric oxide regulates cardiac Ca^{2+} current: involvement of cGMP-inhibited and cGMP-stimulated phosphodiesterases through guanylyl cyclase activation. J Biol Chem 1993;268:26286–95.
24. Gaudiot N, Ribiere C, Jaubert AM, Giudicelli Y. Endogenous nitric oxide is implicated in the regulation of lipolysis through antioxidant-related effect. Am J Physiol 2000;279:C1603–10.
25. Simoncini T, Genazzani AR. Raloxifene acutely stimulates nitric oxide release from human endothelial cells via an activation of endothelial nitric oxide synthase. J Clin Endocrinol Metab 2000;85:2966–9.
26. Gross GJ, Auchampach JA. Blockade of ATP-sensitive potassium channels prevents myocardial preconditioning in dogs. Circ Res 1992;70:223–33.
27. Abe J, Baines CP, Berk BC. Role of mitogen-activated protein kinases in ischemia and reperfusion injury: the good and the bad. Circ Res 2000;86:607–9.
28. Sanada S, Kitakaze M, Papst PJ, et al. Role of phasic dynamism of p38 mitogen-activated protein kinase activation in ischemic preconditioning of the canine heart. Circ Res 2001;88:175–80.
29. Cain BS, Meldrum DR, Meng X, et al. p38 MAPK inhibition decreases TNF-alpha production and enhances postischemic human myocardial function. J Surg Res 1999;83:7–12.
30. Lal AS, Clifton AD, Rouse J, Segal AW, Cohen P. Activation of the neutrophil NADPH oxidase is inhibited by SB 203580, a specific inhibitor of SAPK2/p38. Biochem Biophys Res Commun 1999;259:465–70.
31. Ciesla DJ, Moore EE, Gonzalez RJ, Biffl WL, Silliman CC. Hypertonic saline inhibits neutrophil (PMN) priming via attenuation of p38 MAPK signaling. Shock 2000;14:265–70.
32. Saklatvala J, Rawlinson L, Waller RJ, et al. Role for p38 mitogen-activated protein kinase in platelet aggregation caused by collagen or a thromboxane analogue. J Biol Chem 1996;271:6586–9.
33. Yue TL, Vickery-Clark L, Louden CS, et al. Selective estrogen receptor modulator idoxifene inhibits smooth muscle cell proliferation, enhances reendothelialization, and inhibits neointimal formation in vivo after vascular injury. Circulation 2000;102 Suppl III:281–8.

Early stages of energy transduction by myosin: Roles of Arg in Switch I, of Glu in Switch II, and of the salt-bridge between them

Hirofumi Onishi[†‡], Takashi Ohki[†], Naoki Mochizuki[†], and Manuel F. Morales[§]

[†]Department of Structural Analysis, National Cardiovascular Center Research Institute, Fujishiro-dai, Suita, Osaka 565-8565, Japan; and [§]University of the Pacific, San Francisco, CA 94115

Contributed by Manuel F. Morales, October 7, 2002

On the basis of the crystallographic snapshots of Rayment and his collaborators [Fisher, A. J., Smith, C. A., Thoden, J. B., Smith, R., Sutoh, K., Holden, H. M., & Rayment, I. (1995) *Biochemistry* 34, 8960–8972], we have understood some basic principles about the early stages of myosin catalysis, namely, ATP is drawn into the active site, over which the cleft closes. Catalyzed hydrolysis occurs, and the first product (orthophosphate) is released from the backdoor of the cleft. In the cleft-closing process, the active site incidentally signals its movement to a particular remote tryptophan residue, Trp-512. In this work, we expand on some of these ideas to rationalize the behavior of a mutated system in action. From the behavior of recombinant myosin systems in which Arg-247 and Glu-470 were substituted in several ways, we draw the conclusions that (*i*) the force between Arg-247 and γ-phosphate of ATP may assist in closing the cleft, and incidentally in signaling to the remote Trp, and (*ii*) in catalysis, Glu-470 is involved in holding the lytic H_2O (w_1). We also propose that w_1 and also a second water, w_2, enter into a structure that bridges Glu-470 and the γ-phosphate of bound ATP, and at the same time positions w_1 for its in-line hydrolytic attack.

Research of the last half century established that the free energy of ATP+H_2O, under the influence of the acto-myosin system, degrades in stages while accomplishing external work. The coupled gross movements that we observe are what we call muscle contraction. Underlying such changes are transition: namely, bindings and unbindings of actin or nucleotides, nucleotide hydrolyses, "influence" transmissions, and domain movements, etc. These transitions could not have been probed more deeply without ascertaining the structure of myosin at atomic resolution. This progress was pioneered by Rayment and his collaborators beginning in 1993 (1). Here, we are interested in the events that begin with the binding of ATP to the active site of myosin. In the Trentham–Bagshaw (2, 3) sequence of states, this is the formation of M·ATP.[¶] We are also concerned with the transition to the prehydrolysis state, M*·ATP. Some inferences about the structural changes during these events have already been made by Smith and Rayment (5) based on their "before" and "after" crystallographic snapshots. Specifically, they note that, in the transition state of hydrolysis, Glu-470 pairs with Arg-247 to form a salt-bridge, as a loop (switch II) rotates about a hinge composed of Ile-466, Ala-467, and Gly-468. We have sought to check and enhance their ideas, using the logic that, if these ideas are correct, they should predict the functional behavior of M as it is altered in various site-directed mutations. Our results lead us to suggest that each of the two pairing residues has an important role in early ATP-myosin interaction, and that Glu-470 is probably a key residue in myosin ATP hydrolysis.

Materials and Methods

Protein Preparations. F-actin was prepared from rabbit skeletal muscle as in ref. 6.

Preparation of Recombinant Heavy Meromyosins (HMM). cDNA constructs for wild-type and five mutant (R247A, R247E, E470A, E470R, and R247E/E470R) HMM heavy chains linked to a His tag (at the N terminus) and a myc tag (at the C terminus) were prepared as described in Kojima *et al.* (7). Site-directed mutations were performed by Kunkel's method (8) using various primers (9, 10). Transformation of *Escherichia coli* and production of recombinant baculoviruses were carried out according to the manufacturer's protocol (Life Technologies, Rockville, MD). AcNPV/ELC/RLC viruses (for essential and regulatory light chains) were prepared (11). Expression and purification of recombinant HMMs were carried out (7, 12), except that affinity-purified His-tagged HMMs were further purified by chromatography using a Pharmacia MonoQ column. To remove bound nucleotides from mutant HMMs, the preparation was dialyzed for 2 days against 500 ml of buffer, 0.45 M KCl, 1 mM EDTA, 20 mM Tris·HCl (pH 7.5), and 0.5 mM DTT, on ice with four-time buffer changes.

Fluorimetry and Stopped-Flow Experiments. Fluorimetry was performed with an F-4500 fluorescence spectrophotometer (Hitachi, Tokyo). Stopped-flow experiments were performed with a Hi-Tech Scientific (Salisbury, U.K.) SF61-DX2 stopped-flow spectrophotometer using a 75-W Xe/Hg lamp and a monochromator for excitation wavelength selection. The binding of mant fluorophores to the active site of HMMs was detected by measuring the fluorescence energy transferred from Trp residues to fluorophores. Trp residues were excited at 290 nm, and the emitted light from fluorophores was monitored at 455 nm with a bandwidth of 5 nm (for fluorimetry), or after passing through an LWPF 410-nm filter (Asahi Techno Glass, Tokyo) (for stopped-flow experiments). For Trp fluorescence, excitation was performed at 290 nm, and emission was recorded after passing through a WG 320-nm filter (Schott, Mainz, Germany). Software provided by Hi-Tech was used for curve fitting of the data.

ATPase Assays. The steady-state ATPase activity was measured at 20°C in 0.24 mg/ml HMM, 0.1 mg/ml BSA, 0.45 M KCl, 3 mM $MgCl_2$, 20 mM Tris·HCl (pH 7.5), 0.5 mM DTT, 0.5 mM ATP, and 1 mM EDTA. Actin-activated ATPase activity was measured as a function of actin concentration in 0.054 mg/ml (wild-type) or 0.24 mg/ml (mutants) HMM, 0.04 M KCl, 2 mM $MgCl_2$, 20 mM Tris·HCl (pH 7.5), 0.5 mM DTT, 1 mM ATP, 4 μg/ml chicken gizzard myosin light chain kinase, 1 μg/ml bovine testis calmodulin, and 0.05 mM $CaCl_2$. Released inorganic phosphate was estimated by the malachite green method (13). The activity is per HMM head. Initial phosphate burst was measured as in ref. 9.

Abbreviations: HMM, heavy meromyosin; mantATP, 2′(3′)-*O*-(*N*-methylanthranilloyl) adenosine 5′-triphosphate; w_1, lytic water; w_2, second water.

[‡]To whom correspondence should be addressed. E-mail: honishi@ri.ncvc.go.jp.

[¶]Whereas M is to be read as myosin, the protein used in our work has the sequence of the truncated, doubly headed heavy meromyosin (HMM) extracted from chicken smooth muscle. Myosin exhibits many species differences, but the residues of interest here are highly conserved. The sequence numeration that we use is given in ref. 4. We note that Ser-245, Ser-246, Arg-247, Gly-468, Glu-470, and Trp-512 correspond to Ser-236, Ser-237, Arg-238, Gly-457, Glu-459, and Trp-501 in *Dictyostelium* myosin.

Table 1. Summary of the rate constants and extents for the interaction of nucleotides with wild-type and salt-bridge mutant HMMs

Measurements	Parameters	Wild-type	R247A	R247E	E470A	E470R	R247E/E470R
MantATP binding*	Fast, %	100	82	93	87	58	91
	K_1k_{+2} ($s^{-1}\cdot M^{-1}$)	3.5×10^5	0.49×10^5	0.28×10^5	4.5×10^5	5.7×10^5	2.2×10^5
	Slow, %					33	
	k_{slow}, s^{-1}					0.0001	
Trp fluorescence*	Increase, %	19	1.8	1.1	16	4 (6.7)†	15
	K_1k_{+2} ($s^{-1}\cdot M^{-1}$)	2.5×10^5	0.33×10^5	0.23×10^5	3.1×10^5	4.5×10^5	1.6×10^5
	k_{max}, s^{-1}	166			92		172
	$K_{0.5}$, μM	650			330		980
Phosphate burst*	Mole per mole of HMM head	0.68	0	0	0	0	0
MantATP release*	k_{+3} or $k_{+3}k_{+4}/(k_{+3} + k_{-3})$, s^{-1}	0.009	0.003	0.0011	0.00014	0.000036	0.001
MantADP release*	k_{+5}, s^{-1}	1.3	0.027	0.0036	0.28	0.34	0.031
Steady-state ATPase*	k_{cat}, s^{-1}	0.005	0.002	0.0005	0.00008	0.00003	0.0004
Actin-activated ATPase‡	k_{max}, s^{-1}	1.9	0	0	0	0	0
	K_{actin}, μM	120					

*Conditions: 0.45 M KCl, 3 mM $MgCl_2$, 1 mM EDTA, 20 mM Tris·HCl (pH 7.5) at 20°C.
†The estimated increase for E470R of which sites are vacant.
‡Conditions: 200 μM F-actin, 0.04 mM KCl, 2 mM $MgCl_2$, 20 mM Tris·HCl (pH 7.5) at 25°C.

ATP Detection by HPLC. The amount of ATP in HMM preparations was measured by HPLC (14).

Results and Discussion

Kinetic Scheme for Myosin Mg-ATPase. It has been established (2) that myosin Mg-ATPase can be described by the following minimal reaction scheme:

$$M + T \underset{k_{-1}}{\overset{k_{+1}}{\rightleftharpoons}} M\cdot T \underset{k_{-2}}{\overset{k_{+2}}{\rightleftharpoons}} M^*\cdot T \underset{k_{-3}}{\overset{k_{+3}}{\rightleftharpoons}} M^{**}\cdot D\cdot P_i \underset{k_{-4}}{\overset{k_{+4}}{\rightleftharpoons}} M^*\cdot D \underset{k_{-5}}{\overset{k_{+5}}{\rightleftharpoons}} M + D$$

where M is myosin, and T, D, and P_i are ATP, ADP, and inorganic phosphate, respectively. k_{+i} and k_{-i} are forward and backward rate constants, respectively. The single and double asterisks (* and **) refer to different conformations as detected by intrinsic protein fluorescence. Step 1 corresponds to the formation of a collision complex of myosin and ATP. Binding of ATP is followed by a conformational change (step 2), and, subsequently, ATP is hydrolyzed (step 3). The produced P_i and ADP are released from the ternary complex in steps 4 and 5, respectively. In the wild-type system, steps 1, 2, and 3 are fast, and step 4 rate limits the overall reaction. Here, in analyzing the Mg-ATPase of myosin mutants, we used the foregoing reaction scheme with selected rate constants. An *assumption* is that differences between the behavior of wild-type and mutant systems are expressible solely as differences in rate constants, keeping the reaction connectivities the same.

Binding of mantATP to HMMs. To detect binding of nucleotides by wild-type and mutant HMMs, we used a fluorescent nucleotide [2′(3′)-*O*-(*N*-methylanthranilloyl) adenosine 5′-triphosphate (mantATP)]. Because the excitation spectrum of mant fluorophores closely overlaps the emission spectrum of Trp residues, the observed fluorescence is energy transferred from Trp residues to fluorophores bound at the active site of HMMs. Addition of excess mantATP produced increases in fluorescence of 82%, 93%, 87%, 58%, and 91% for R247A, R247E, E470A, E470R, and R247E/E470R mutants, respectively, compared with 100% for wild-type (denoted as "fast" in Table 1). In each of these HMMs, the fluorescence-time transient was well fitted by a single exponential curve. The observed rate constants (k_{obs}) were linearly dependent on the mantATP concentration, in the range from 5 to 60 μM (Fig. 1). The slope of the plots of k_{obs} against [mantATP] depends on the occupants of positions 247 and 470. The second-order rate constant (K_1k_{+2}) of nucleotide binding was greatly decreased for R247A, and decreased even more for R247E, whereas it was slightly increased for E470A and increased more for E470R (Table 1). We explain these results by assuming that γ-phosphate occupies a position closer to position 247 than to position 470. For R247E/E470R, K_1k_{+2} was close to that of wild type (Table 1). Therefore, we think that, in the inverted arrangement, γ-phosphate moves to interact with R at 470.

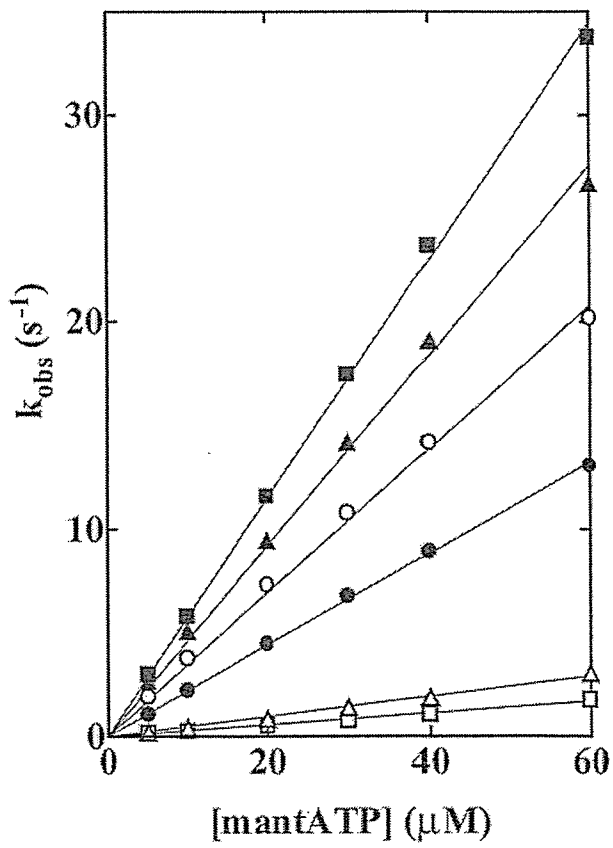

Fig. 1. Rates of binding of mantATP to wild-type and mutant HMMs. Various concentrations of mantATP were mixed with 0.56 μM HMMs in a rapid mixing stopped flow fluorometer, and the increases in the energy transfer from Trp residues to bound mantATP were recorded. Observed rate constants k_{obs} were plotted as a function of the mantATP concentration. The slope of the plots of k_{obs} vs. [mantATP] are the second-order rate constants of mantATP binding (K_1k_{+2}) and are listed in Table 1. HMMs: Wild-type (○), R247A (△), R247E (□), E470A (▲), E470R (■), and R247E/E470R (●). Conditions: 0.45 M KCl, 3 mM $MgCl_2$, 1 mM EDTA, 20 mM Tris·HCl (pH 7.5) at 20°C.

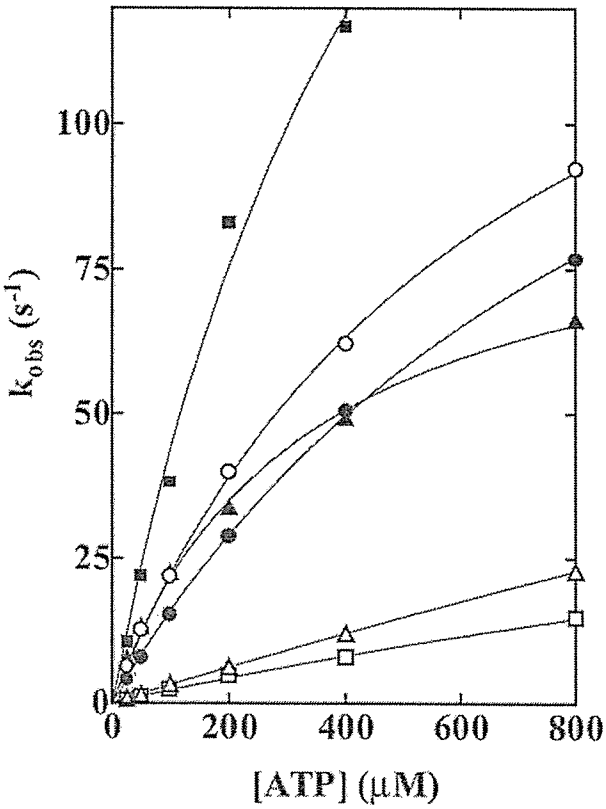

Fig. 2. Rates of increases in Trp fluorescence of wild-type and mutant HMMs on addition of ATP. HMMs (0.56 μM) were mixed with various concentrations of ATP in a rapid mixing stopped-flow fluorometer, and the increases in the Trp fluorescence were recorded. Observed rate constants k_{obs} were plotted as a function of the ATP concentration. The slopes of the regressions to the linear portions at lower ATP concentrations are the second-order rate constants of ATP binding (K_1k_{+2}). The plot was well described by a hyperbola [$k_{obs} = k_{max}[ATP]/([ATP] + K_{0.5})$]. k_{max} is the predicted value for k_{obs} at infinite [ATP] and $K_{0.5}$ is the ATP concentration in which $k_{obs} = k_{max}/2$. K_1k_{+2}, k_{max}, and $K_{0.5}$ are listed in Table 1. HMMs: Wild-type (○), R247A (△), R247E (□), E470A (▲), E470R (■), and R247E/E470R (●). Conditions: 0.45 M KCl, 3 mM $MgCl_2$, 1 mM EDTA, and 20 mM Tris·HCl (pH 7.5) at 20°C.

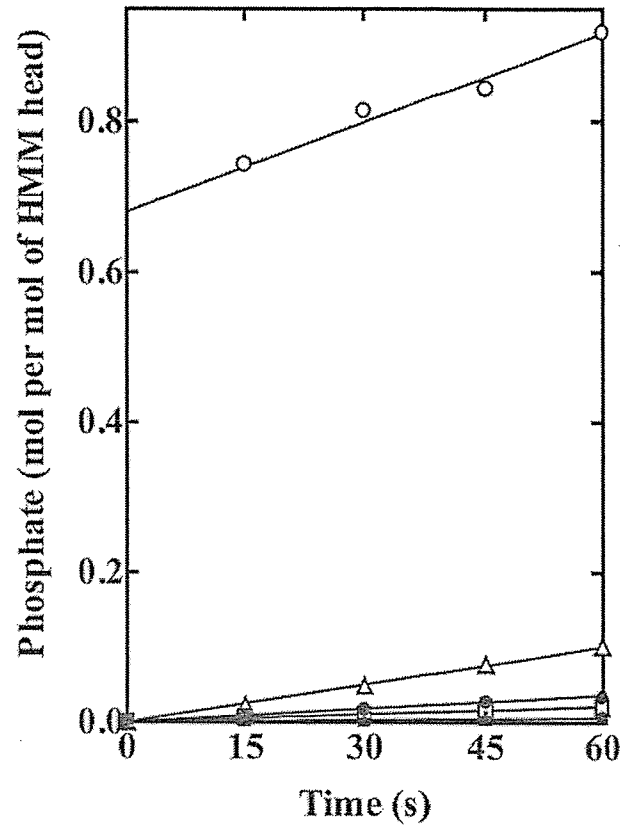

Fig. 3. Initial P_i bursts in the hydrolysis of ATP by wild-type and mutant HMMs. Assay conditions were 0.20 mg/ml of each of wild-type (○), R247A (△), R247E (□), E470A (▲), E470R (■), and R247E/E470R (●) HMMs, 0.45 M KCl, 3 mM KCl, 1 mM EDTA, 20 mM Tris·HCl, pH 7.5, 0.5 mM DTT, and 4 μM [γ-^{32}P]ATP. The data of wild-type HMM were cited from ref. 10. The burst size, determined by extrapolating the steady-state P_i release to zero time, was 0.68 moles of P_i per mole of HMM head for the wild-type HMM, but no burst was obtained for any of the mutant HMMs.

It should be noted that E470R shows a slow transient of fluorescence increase (denoted as "slow" in Table 1). In that way, the fluorescence increase of this mutant produced by adding mantATP finally reached 91% of the value obtained with wild type. In contrast to the faster one, the rate of the slower component was independent of the mantATP concentration (data not shown). This behavior was also very similar to that in a single turnover of mant fluorophore recorded on chasing with excess ATP. Moreover, analysis by reverse-phase HPLC revealed that E470R contains about one-third mole of ATP per mole of head (data not shown). Therefore, we can assume that some of the enzyme sites of E470R are occupied with ATP. This result suggests that the slow rate of mantATP binding is due to the slow release of nonfluorescent occupants from enzyme sites.

Increase in Trp Fluorescence of HMMs by Binding of ATP. Myosins respond to binding of ATP with an increase in intrinsic protein fluorescence. Several studies (12, 15–17) have suggested that Trp-512 (of smooth muscle myosin) is the responsible Trp residue. Crystallographic studies demonstrated that the ATP-induced rotation of the lower piece of 50 kDa, which bears Trp-512 at its tip, can perturb this fluorophore (5). Here, we took the increase in Trp fluorescence as an indicator of the rotation of the 50-kDa lower piece, the rotation being presumably equivalent to the transition from the "open" to the "closed" state identified in crystallography. The maximum increase in Trp fluorescence depends strongly on the occupants of positions 247 and 470. The addition of excess ATP increased the Trp fluorescence by 1.8%, 1.1%, 18%, 4%, and 15% in the case of R247A, R247E, E470A, E470R, and R247E/E470R, respectively, compared with 19% for wild type (Table 1). These results suggest that R at 247 is the most important residue for the open → closed transition occurring in step 2, but that in the inverted arrangement, R at 247 is functionally replaceable by R at 470. As described above, the E470R used had one-third of its enzyme sites occupied with ATP. Therefore, the real increase in Trp fluorescence might have been as large as 6.7%, still smaller than the value for wild type. We explain this result by assuming that a repulsive strain between two R residues at 247 and 470 partially interferes with the open-closed transition.

Trp fluorescence-time transients were well fitted by a single exponential. The observed rate constants were linearly dependent on the concentration of ATP at low ATP concentrations (Fig. 2). K_1k_{+2} can be obtained for the rate of developing Trp fluorescence as well as the rate of developing mantATP fluorescence (Table 1). The numbers are very similar for both. These results support our assumption that the position of γ-phosphate of bound ATP is closer to position 247 than to position 470. At higher ATP concentrations, k_{obs} was no longer linearly dependent on the ATP concentration.

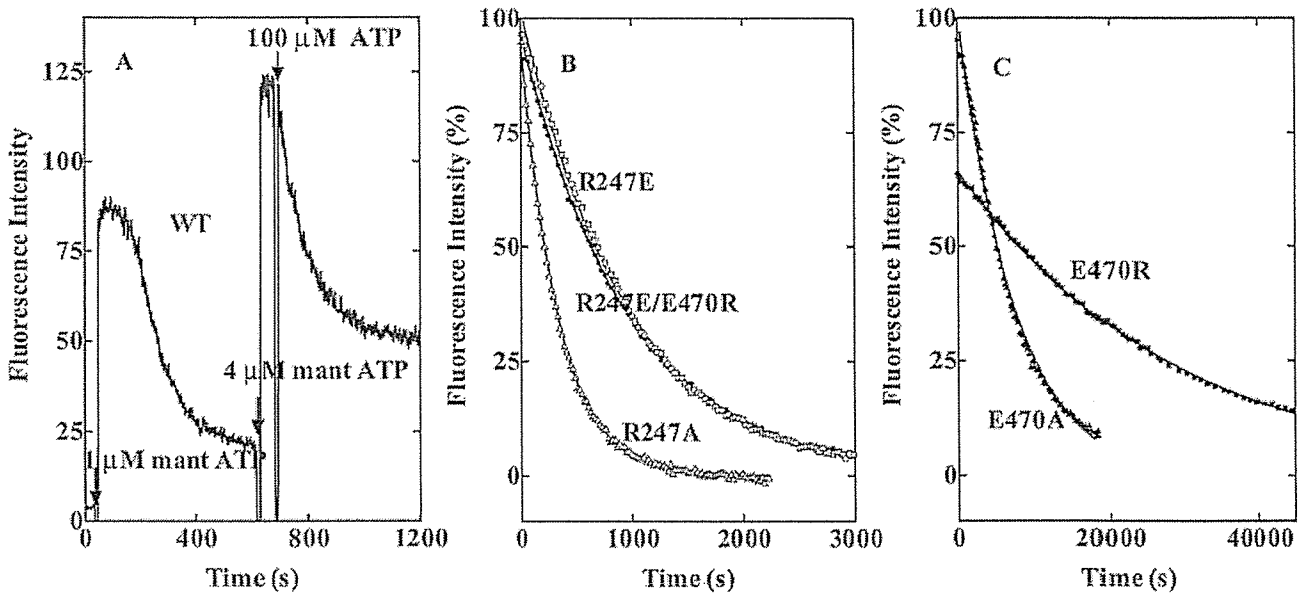

Fig. 4. Turnover rates of fluorescent intermediates measured by the decay of fluorescence from wild-type HMM– and mutant HMM–mantATP complexes on addition of excess ATP. (*A*) MantATP (1 and 4 μM) was added to 0.56 μM wild-type HMM at the arrows labeled with 60 and 530 s, respectively. Increasing fluorescence was used to monitor nucleotide binding to the enzyme sites. At 600 s, 100 μM nonfluorescent ATP was added to the reaction mixture. Because there is no longer any "new" mantATP that can bind to enzyme sites, the rate of decrease in fluorescence is expressed by the turnover rate of the fluorescent intermediate. (*B* and *C*) Decays of the fluorescences from mant fluorophores bound to mutants on adding excess ATP. MantATP (1 μM) was added to 0.56 μM HMMs (△, R247A, □, R247E, and ●, R246E/E470R, in *B*; and ▲, E470A, and ■, E470R, in *C*), bringing the system to a high, maintained fluorescence level. While in the steady state, 100 μM ATP was added (at time 0). This addition causes the fluorescence to start decaying. The continuous lines are the best fits to single exponential decays. Numerical values of k_{obs} are listed in Table 1. Conditions: 0.45 M KCl, 3 mM $MgCl_2$, 1 mM EDTA, 20 mM Tris·HCl (pH 7.5), and 0.5 mM DTT, at 20°C.

The plots of k_{obs} against [ATP] were well described by hyperbolas, $k_{obs} = k_{max}$ [ATP]/([ATP] + $K_{0.5}$). The maximum rates (k_{max}) of 166 s^{-1}, 92 s^{-1}, and 172 s^{-1} were obtained for wild type, E470A, and R247E/E470R, respectively (Table 1). In wild type, the transition from M*·T to M**·D·P_i (step 3) is also fast. Although the maximum rate of this transition could not be obtained from P_i measurements, we assigned to k_{max} of the fluorescence signal the rate constant of step 2, (k_{+2} + k_{-2}), because the fluorescence signal showed no deviation from a single exponential curve. Because E470A and R247E/E470R have very slow transitions from M*·T to M**·D·P_i (see Fig. 3), we suggest that k_{max} definitely corresponds to k_{+2} + k_{-2}.

Initial P_i Burst in ATP Hydrolysis. Hydrolysis of ATP by wild type occurs rapidly, and results in a metastable ternary complex between myosin, ADP, and P_i. When the ATPase reaction is quickly terminated by acid, a stoichiometric P_i burst is obtained (18). Previously, we have found that the burst size in wild type was 0.68 moles per mole of HMM head, whereas four single mutants (R247A, R247E, E470A, and E470R) exhibited no P_i burst (9, 10). In the same paper, we also reported that the burst size of R247E/E470R was quite similar to that of wild type. Later, however, we discovered that, due to a labeling mistake, the mutant that we described as the double mutant was actually P548G (19). When we reexamined, using the authentic double mutant, we found that no burst at all was generated by the true double mutant. In the inverted arrangement, the ability to form the salt-bridge did not *per se* restore normal ATP hydrolysis. These results clearly show that hydrolysis does not always accompany the open → closed transition measured by the ATP-induced increase in Trp fluorescence. Earlier work (9, 10) and also the present work show that R247A, R247E, E470A, E470R, and R247E/E470R exhibit no P_i burst, but do exhibit the ATP-induced increase in Trp fluorescence, so we must assume that, in such cases, [M*·T] is greater than [M**·D·P_i], i.e., the equilibrium constant for step 3 (K_3) is much smaller than 1. For rabbit skeletal subfragment 1, it was found that K_3 = ≈10 (100 mM KCl, pH 7.0, 20°C; ref. 2).

Turnover of Fluorescent Intermediates in the mantATP Hydrolysis. Fig. 4*A* shows time-dependent changes in mant fluorescence on sequential additions of mantATP and ATP to wild-type HMM. We can assume that the high, constant phase represents saturation of the enzyme sites with fluorophores. When 1 μM mantATP was added, this phase was followed by a phase in which fluorescence was decreasing. This decrease can be taken to measure the diminishing fraction of sites that are occupied by fluorophore. When 4 μM mantATP was added, the high, constant phase became longer. After maximal mantATP binding, the HMM–mantATP complex was then mixed with 100 μM nonfluorescent ATP, which took over all vacant sites. Because, according to the kinetic scheme (2, 3), the P_i release step (step 4) is rate-limiting, the decay of mant fluorescence on adding excess ATP is an indirect measure of the single turnover rate of ATP hydrolysis. A rate constant of 0.009 s^{-1} for k_{+4} was obtained by this measure. The time course of the decay in fluorescence after adding excess ATP was rather similar to that of the decrease in fluorescence after adding 1 μM mantATP.

In mutants, because step 3 is very slow, the rate constant of decay of mant fluorescence on addition of 100 μM ATP is not as simple as it is in wild type. Its value is k_{+3} if $k_{+3} < k_{+4}$ and $k_{+3}k_{+4}/(k_{+3} + k_{-3})$ if $k_{+3} > k_{+4}$. Fig. 4 *B* and *C* shows that this rate constant depends on occupants at positions 247 and 470, but the dependency is very different from either the K_1k_{+2} of nucleotide binding (Figs. 1 and 2, and Table 1), or the ATP-induced increase in Trp fluorescence (Table 1). The rates for R247A and R247E were reduced 3- and 9-fold, respectively, compared with wild type, but those for E470A and E470R were reduced by 65- and 225-fold, respectively. The especially slow rate for mutants at position 470 suggests that the charge change

(− to 0, or − to +), or perhaps the replacement of a carbonyl group at 470, is very significant in inhibiting hydrolysis. The rate of decay in mant fluorescence in R247E/E470R (Fig. 4*B*) was 25-fold faster than that in E470R, but its rate was 9-fold slower than in wild type. We can assume that either the second charge change (R247E) or the ability to form the inverted salt-bridge partially restores the steady-state ATP hydrolysis, but never as well as in the wild-type arrangement.

MantADP Removal from HMM-mantADP Complexes. The rate of ADP removal from M*·D (step 5) was measured by displacing mantADP from HMM–mantADP complexes with excess ATP. The rate of the decrease in fluorescence expresses the rate of removal of mantADP. If the rate of mantADP removal is faster than the rate of removal of earlier steps, we conclude that removal of bound ADP cannot be the overall rate-limiting step in the sequence. When 100 μM ATP was added to a prepared mixture of 0.56 μM HMMs and 2 μM (for mutants) or of 10 μM (for wild type) mantADP, the plots of transient decreases against time of fluorescence could be fitted by single exponentials. The observed rate constants of mantADP removal (k_{+5}) were 1.3 s^{-1} for wild type, 0.027 s^{-1} for R247A, 0.0011 s^{-1} for R247E, 0.28 s^{-1} for E470A, 0.34 s^{-1} for E470R, and 0.031 s^{-1} for R247E/E470R, respectively (Table 1). In wild type, the rate of removal of mantADP by adding excess ATP was much faster than the rate of mant fluorescence decrease when the initial substrate was mantATP (see Fig. 4), supporting the established conclusion that the rate-limiting step in the steady state is the transition from M**·D·P_i to M*·D (step 4), rather than the removal of ADP from M*·D (step 5). In two of the single mutants, R247A and R247E, the rates at which mant fluorescence decreases, when the initial substrates were mantADP and mantATP, were still different, but much nearer to one another (the ratio of the former vs. the latter was 9 for R247A and 3 for R247E, compared with 140 for wild type). Interestingly, two other single mutants showed opposite effects, being the ratio of 2,000 for E470A and 8,500 for E470R. Again, this observation supports our idea that Arg at 247 and Glu at 470 have different roles in the ATP hydrolysis.

Steady-State ATP Hydrolysis. From experiments consisting of chasing bound mant fluorophores by excess ATP, we can identify any one of several intermediates that can be only slowly removed. To decide whether the step determined by chase experiments is rate-limiting in the cycle of ATP hydrolysis, we performed steady-state measurements of ATPase at 0.5 mM ATP. The steady-state ATPase activity (k_{cat}) was 0.005 s^{-1} for wild type, 0.002 s^{-1} for R247A, 0.0005 s^{-1} for R247E, 0.00008 s^{-1} for E470A, 0.00003 s^{-1} for E470R, and 0.0004 s^{-1} for R247E/E470R (Table 1). Because the dissociation constant of HMMs for ATP is much less than 0.5 mM, the observed rates are maximal at saturating ATP concentration. When compared at the corresponding HMMs, the k_{cat} values and the rates of decay of mant fluorescence on adding excess ATP to HMM-mantATP complexes were very similar. Therefore, we can conclude that the decay of mant fluorescence in chase experiments is limited by whatever is the slowest step in the ATPase cycle.

Actin activated the ATPase activity of wild-type HMM, yielding a maximum rate of 1.9 s^{-1} and an apparent dissociation constant of 120 μM for actin. Previous kinetic studies on rabbit skeletal acto-subfragment 1 ATPase showed that actin primarily accelerates the step of releasing inorganic phosphate from M**·D·P_i. If any one of earlier steps is limited by mutations, we would not observe actin activation. To examine whether salt-bridge mutants are such a case, we measured the steady-state ATPase activity in the presence of 200 μM [actin]. Practically no actin activation was observed in any of the mutant cases (Table 1). These results are consistent with our observation that the rate of hydrolysis of bound ATP (step 3) is strongly limited in these mutations (Fig. 3).

Possible Roles of R247, E470, and the Salt-Bridge in ATP Hydrolysis. In this work, we take a rapid increase in fluorescence emission from HMM as evidence that, on binding at the active site, an influence quickly travels from the site to a particular residue, Trp-512 (12, 15–17). In the case in which a mant fluorophore has access to the active site, under illumination at 290 nm, we take a rapid increase in fluorescence at 455 nm as evidence that the fluorophore is more or less statically bound to the active site (assuming that such a fluorophore is tuned only to accept energy from Trp and then re-emit it at 455 nm), but we do not claim to know the identity of the originating Trp.

From the successive crystallographic snapshots by Rayment and his colleagues (5, 20), we have gained an insight into the events after the binding of ATP to the active site of myosin: The cleft closes, and Arg-247 and Glu-470, once long separated, come together into a salt-bridge. In this process, Arg-247 comes to lie close to the γ-phosphate of the bound ATP, as does Glu-470. Simultaneously, these effects are transmitted toward Trp-512. Also, in some hitherto unexplained way, a water molecule at a particular location is prepared to attack the P-O-P bridge of ATP. After the bridge severance, the cleft reopens and orthophosphate is released from the back door of the cleft.

In the present work, we find that, even after making substantial structural substitutions by site-directed mutation, we can continue to track in time various functional parameters. Specifically, these are the rate and extent at which mant-ATP occupies the active site, the rate and extent at which signals from the active site reach Trp-512, and the rate at which bound ATP is hydrolyzed. When we measure these parameters in various mutants, we find a very interesting pattern of results (Table 1). We denote paired mutations at the salt-bridge positions as 247 and 470, and identify RE as wild-type; we have also studied AE, EE, RA, RR, and ER. A simple and very good correlation is found between the presence of R and

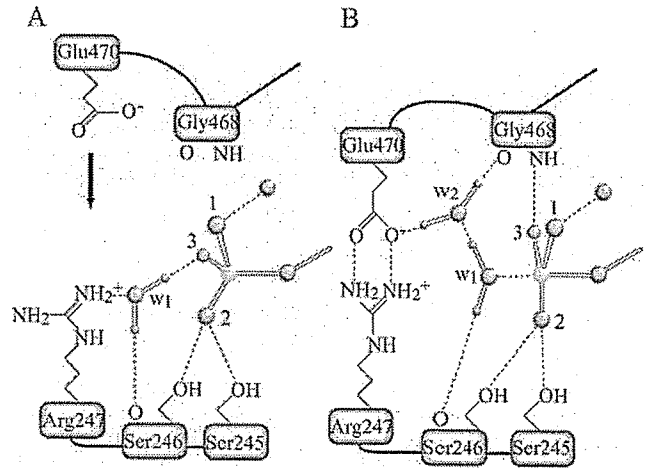

Fig. 5. Schematic representation of the γ-phosphate pocket of the pre-hydrolytic state (*A*) and of the transition state for hydrolysis (*B*). In the former, the γ-phosphate of ATP is in a tetrahedral arrangement with its four oxygen atoms, whereas, in the latter, five oxygen atoms bound to the γ-phosphate adopt a trigonal bipyramidal arrangement. Two water molecules involved in hydrogen bonding are denoted as w_1 and w_2. We assume that w_1 in *A* is HOH1181 in the Fisher *et al.* structure (ref. 20; Protein Data Bank ID code 1MMD), and that w_1 and w_2 in *B* take the place of the terminal oxygen of the vanadate moiety and that of HOH697, respectively, in the Smith and Rayment structure (ref. 5; Protein Data Bank ID code 1VOM). Only those stereochemical interactions that participate in positioning w_1, w_2, and three oxygen atoms (labeled 1, 2, and 3) of the γ-phosphate are depicted. Covalent bonds are shown as solid lines and hydrogen bonds and ionic interactions in dashed lines. Phosphorus, oxygen, hydrogen, and magnesium are depicted in yellow, red, violet, and green, respectively.

the rate of occupation of the active site by a mant analog. Similarly there is a good correlation between influences reaching Trp-512 and the presence of R. On the other hand, there is a strong correlation between catalyzed hydrolysis of ATP and the presence of E. Lastly, it is evident that occupation of the active site, and perturbation of Trp-512, can both occur without hydrolysis (e.g., RA). Translating these results into tentative conclusions, we suggest that, as surmised by Smith and Rayment (5), Arg-247 and Glu-470 certainly have important functions in forming a salt-bridge. In our view, the electrical force between Arg-247 and the γ-phosphate of the ATP bound to the active site, although attenuated in solution, is probably significant for cleft closure; this closure is required to form the salt-bridge. If some other force, e.g., interactions between the P-loop and the triphosphate moiety of the ATP, is involved in the cleft closure, the long-range force between R and the γ-phosphate would at least stabilize the closed interaction. In anomalous circumstances, closure can occur without hydrolysis. Also, in the present work, the tight correlation between hydrolysis and the presence of E leads us to revive our old hypothesis that Glu-470 *per se* is involved in catalyzing the hydrolysis (9). Formation of the salt-bridge would move Glu-470 to obligatorily participate in the catalysis. In the cases of AE and RA, the reasons for failing to catalyze properly would be different. In the case of AE, closure is poor and E does not move to the proper position, whereas in the case of RA, closure occurs, but E is lost.

Our results, reported above, raise the question as to how the two residues, Arg-247 and Glu-470, can interact specifically with a bound γ-phosphate separated by >5 Å, and why crystallography reveals no amino acid side chain in the γ-phosphate pocket that is near enough to the phosphate to function as the catalytic base in hydrolysis. Building on the reports of Fisher *et al.* (20) and of Smith and Rayment (ref. 5, discussion about plasticity conferred on the γ-phosphate pocket by hydrogen bonding), and on our present results, we speculate about the mechanism of myosin catalysis. We suppose that two water molecules are involved, the lytic water, w_1, and also a second water, w_2. In the structure of the MgADP·BeF_x complex that mimics the prehydrolysis state, M·T, w_1 is hydrogen-bonded to a fluoride of BeF_x and to the main-chain carbonyl oxygen of Ser-246 (Fig. 5*A*). w_1 also interacts electrostatically with the guanydyl group of Arg-247. We propose that Arg-247 thus indirectly interacts with γ-phosphate via this water, and so, for this reason, Arg-247 is important in nucleotide binding to the active site, and in inducing cleft closure. On the other hand, in the same motor domain, but now with MgADP·vanadate (which mimics the transition state to M**·D·P_i), w_2 appears in the phosphate pocket (see Fig. 5*B*). w_2 is hydrogen-bonded to the main-chain carbonyl oxygen of Gly-468 and to one of the two oxygen atoms in the carboxyl group of Glu-470. This finding suggests that, after cleft closure, movement of Glu-470 results, first, in bridging it to Arg-247, then in releasing w_1 from Arg-247, and, finally, in bonding of the two hydrogen atoms of w_1 with the oxygen atom of w_2 and with the main-chain carbonyl oxygen of Ser-246. Then, the conformation becomes optimal, orienting w_1 for a nucleophilic attack on the γ-phosphorus. The two hydrogen atoms of w_2 are oriented toward the carboxyl group of Glu-470 and to the main-chain carboxyl oxygen of Gly-468. These oxygen atoms seem to function as proton acceptors, so we can speculate that w_2 accepts a proton from w_1, after w_1 has made its attack on the γ-phosphorus (see Fig. 5*B*). Alternatively, the hydrogen bond network around w_1 may stabilize a trigonal-bipyramidal arrangement of oxygen atoms around the γ-phosphorus in the transition state.

The structures found by Rayment harmonize well with our reported correlation between the presence of E in the salt-bridge and the ability of the system to catalyze hydrolysis. The inverted mutant, R247E/E470R, supports a fluorescence enhancement of ≈80% of that in a wild-type system, but not a phosphate burst. Presumably this result is because the influence of R on the γ-phosphate is long-ranged, whereas the positioning of w_2 in the catalytic apparatus has to be precise. In other hydrolyzing systems, e.g., G-proteins, the lytic water is required to move to an in-line position (21–24). Perhaps, in myosin catalysis, the Glu-470-w_2-Gly-468 network plays the role that the catalytic Gln plays in G-proteins. In the interesting simulations of Okimoto *et al.* (25) about events in ATPase, obligatory participation is assigned to Glu-470. However, the simulations do not take explicit account of w_2; perhaps for that reason, they deduce an unusually large energy of activation.

In wild-type myosin, formation of M**·D·P_i is very fast compared with release of the produced P_i, so this intermediate accumulates when the system is in the steady state. A reasonable speculation for the slowness with which P_i is released is that the release corresponds to the cleft reopening, and that such a process takes time. Neither AE nor EE exhibits a P_i burst. This result suggests that [M**·D·P_i] is very small, even though the mutants achieve an ATPase activity comparable to that of the wild-type system. In our view, this result would mean that, in these mutants, either the cleft reopens faster or it never closes well. Recently, Manstein and colleagues (26) found that, in *Dictylstelium*, with the mutation corresponding to EE, the cleft remains open, even in the presence of the tightly binding nucleotide analog, MgADP·BeF_x. Our speculation seems to be consistent with their finding.

We close with a technological note. Mutants such as RR, in which M*·T is highly stabilized (presumably by overattraction to γ-phosphate), are very difficult to purify by dialysis, and for that reason they exhibit properties that are easy to misinterpret.

We are grateful to Professor H. M. Martinez for his important counsel and Professors T. Burghardt, I. Rayment, and J. T. Pearson for significant improvements in our manuscript. This work was supported by Grant-in-Aids for Scientific Research and by Special Coordination Funds for Promoting Science and Technology from the Ministry of Education, Culture, Sports, Science, and Technology (to H.O. and N.M.) and by Grant MCB 9603670 from the National Science Foundation (to M.F.M.).

1. Rayment, I., Rypniewski, W. R., Schmidt-Bäse, K., Smith, R., Tomchick, D. R., Benning, M. M., Winkelmann, D. A., Wesenberg, G. & Holden, H. M. (1993) *Science* **261**, 50–58.
2. Bagshaw, C. R. & Trentham, D. R. (1974) *Biochem. J.* **141**, 331–349.
3. Bagshaw, C. R., Eccleston, J. F., Eckstein, F., Goody, R. S., Gutfreund, H. & Trentham, D. R. (1974) *Biochem. J.* **141**, 351–364.
4. Yanagisawa, M., Hamada, Y., Katsuragawa, Y., Imamura, M., Mikawa, T. & Masaki, T. (1987) *J. Mol. Biol.* **198**, 143–157.
5. Smith, C. A. & Rayment, I. (1996) *Biochemistry* **35**, 5404–5417.
6. Spudich, J. A. & Watt, S. (1971) *J. Biol. Chem.* **246**, 4866–4871.
7. Kojima, S., Fujiwara, K. & Onishi, H. (1999) *Biochemistry* **38**, 11670–11676.
8. Kunkel, T. A., Roberts, J. D. & Zakour, R. A. (1987) *Methods Enzymol.* **154**, 367–382.
9. Onishi, H., Morales, M. F., Kojima, S., Katoh, K. & Fujiwara, K. (1997) *Biochemistry* **36**, 3767–3772.
10. Onishi, H., Kojima, S., Katoh, K., Fujiwara, K., Martinez, H. M. & Morales, M. F. (1998) *Proc. Natl. Acad. Sci. USA* **95**, 6653–6658.
11. Onishi, H., Maéda, K., Maéda, Y., Inoue, A. & Fujiwara, K. (1995) *Proc. Natl. Acad. Sci. USA* **92**, 704–708.
12. Onishi, H., Konishi, K., Fujiwara, K., Hayakawa, K., Tanokura, M., Martinez, H. M. & Morales, M. F. (2000) *Proc. Natl. Acad. Sci. USA* **97**, 11203–11208.
13. Kodama, T., Fukui, K. & Kometani, K. (1986) *J. Biochem. (Tokyo)* **99**, 1465–1472.
14. Samizo, K., Ishikawa, R., Nakamura, A. & Kohama, K. (2001) *Anal. Biochem.* **293**, 212–215.
15. Johnson, W. C., Jr., Bivin, D. B., Ue, K. & Morales, M. F. (1991) *Proc. Natl. Acad. Sci. USA* **88**, 9748–9750.
16. Hiratsuka, T. (1992) *J. Biol. Chem.* **267**, 14949–14954.
17. Batra, R. & Manstein, D. J. (1999) *Biol. Chem.* **380**, 1017–1023.
18. Kanazawa, T. & Tonomura, Y. (1965) *J. Biochem. (Tokyo)* **57**, 604–615.
19. Onishi, H., Kojima, S., Katoh, K., Fujiwara, K., Martinez, H. M. & Morales, M. F. (2001) *Proc. Natl. Acad. Sci. USA* **98**, 5369a.
20. Fisher, A. J., Smith, C. A., Thoden, J. B., Smith, R., Sutoh, K., Holden, H. M. & Rayment, I. (1995) *Biochemistry* **34**, 8960–8972.
21. Pai, E. F., Krengel, U., Petsko, G. A., Goody, R. S., Kabsch, W. & Wittinghofer, A. (1990) *EMBO J.* **9**, 2351–2359.
22. Coleman, D. E., Berghuis, A. M., Lee, E., Linder, M. E., Gilman, A. G. & Sprang, S. R. (1994) *Science* **265**, 1405–1412.
23. Sondek, J., Lambright, D. G., Noel, J. P., Hamm, H. E. & Sigler, P. B. (1994) *Nature* **372**, 276–279.
24. Schweins, T., Geyer, M., Scheffzek, K., Warshel, A., Kalbitzer, H. R. & Wittinghofer, A. (1995) *Nat. Struct. Biol.* **2**, 36–44.
25. Okimoto, N., Yamanaka, K., Ueno, J., Hata, M., Hoshino, T. & Tsuda, M. (2001) *Biophys. J.* **81**, 2786–2794.
26. Kliche, W., Fujita-Becker, S., Kollmar, M., Manstein, D. J. & Kull, F. J. (2001) *EMBO J.* **20**, 40–46.

THE JOURNAL OF BIOLOGICAL CHEMISTRY
Vol. 277, No. 46, Issue of November 15, pp. 43771–43777, 2002
Printed in U.S.A.

Expression of Calcineurin B Homologous Protein 2 Protects Serum Deprivation-induced Cell Death by Serum-independent Activation of Na^+/H^+ Exchanger*

Received for publication, August 14, 2002, and in revised form, September 10, 2002
Published, JBC Papers in Press, September 10, 2002, DOI 10.1074/jbc.M208313200

Tianxiang Pang‡, Shigeo Wakabayashi§, and Munekazu Shigekawa

From the Department of Molecular Physiology, National Cardiovascular Center Research Institute, Fujishiro-dai 5-7-1, Suita, Osaka 565-8565, Japan

The calcineurin B homologous protein (designated CHP1) has been shown to be a common essential cofactor for the plasma membrane Na^+/H^+ exchangers (NHEs) (Pang, T., Su, X., Wakabayashi, S., and Shigekawa, M. (2001) *J. Biol. Chem.* 276, 17367–17372). In this study, we characterized the function of another isoform of CHP (designated CHP2) that has a 61% amino acid identity with CHP1. CHP2, like CHP1, conferred the ability to NHEs 1–3 to express a high exchange activity by binding to the juxtamembrane region of the cytoplasmic domain of the exchanger, but it interacts more strongly (~5-fold) with NHE1 than does CHP1. Although CHP1 is expressed ubiquitously at relatively high levels, CHP2 expression was extremely low in most human tissues but was higher in tumor cells. We produced stable cell clones overexpressing either CHP1 or CHP2 in which one of them is predominantly bound to NHE1. Serum (10%) induced a significant cytoplasmic alkalinization (0.1–0.2 pH unit) in cells co-expressing CHP1 and NHE1 but not in cells co-expressing CHP2 and NHE1. In the latter, pH_i was high (7.4–7.5) even in the absence of serum, suggesting that NHE1 was already activated. Surprisingly, most (>80%) of CHP2/NHE1 cells unlike CHP1/NHE1 cells were viable even after long serum starvation (>7 days). Thus, the expression of CHP2 appears to protect cells from serum deprivation-induced death by increasing pH_i. These properties of CHP2/NHE1 cells are similar to those of malignantly transformed cells. We propose that serum-independent activation of NHE1 by bound CHP2 is one of the key mechanisms for the maintenance of high pH_i and the resistance to serum deprivation-induced cell death in malignantly transformed cells.

The Na^+/H^+ exchanger (NHE)[1] is an electroneutral countertransporter that catalyzes H^+ extrusion coupled to Na^+ influx across the biological membranes. The NHE family consists of at least seven isoforms that are different in tissue or subcellular localization (1–3). The ubiquitous NHE1 isoform plays a major role in intracellular pH (pH_i) homeostasis and cell volume regulation (1–3) and has extensively been studied in terms of its structure, function, and regulatory mechanism. An outstanding feature of NHE1 is that it is activated in response to various extracellular stimuli including hormones, growth factors, cytokines, and mechanical stress such as cell shrinkage, resulting in cytoplasmic alkalinization in the absence of bicarbonate (1–4). In the NHE1 regulation by these stimuli, the involvement of a variety of signaling molecules (*i.e.* calcineurin B homologous protein (5, 6), Ca^{2+}/calmodulin (7–9), low molecular weight GTPases Ras and Rho (10–12), p42/44 mitogen-activated protein kinases (13), p90 ribosomal S6 kinase (14), 14-3-3 protein (15), Nck-interacting kinase (16), and phosphatidylinositol 4,5-bisphosphate (17) has been reported. However, the interrelations among the functions of these signaling molecules leading to the NHE1 activation have not yet been well sorted out.

It has often been documented that the increased pH_i caused by NHE1 activation serves as a permissive or an obligatory signal for cell proliferation and differentiation (1–4, 18, 19). Oppositely, the decreased pH_i attributed to reduced NHE1 activity has been shown to result in growth arrest or cell death (20–23). Furthermore, the activation of NHE1 has often been associated with oncogenic transformation (24–28). For example, cells transformed by *ras* oncogene (25–27) or E7 oncogene from papillomavirus type 16 (28) have been shown to maintain high pH_i in the absence of serum with an accompanying high activity of NHE1, which may be one of key factors involved in abnormal cell growth or enhanced cell invasion. However, molecular mechanisms underlying these phenotypic alterations remain poorly understood.

Recently, we have provided evidence that calcineurin B homologous protein (CHP1) serves as an essential cofactor, which is required for at least three NHE isoforms, NHEs 1–3, to express high physiological levels of exchange activity because CHP1 deprivation results in dramatic reductions (>90%) of activity (6). However, it is not clear how CHP1 is involved in the regulation of NHEs in response to the extracellular stimuli. There is another human CHP isoform (CHP2) that was identified in human cancer patient (NCBI nucleotide accession number NM_022097 with designation of hepatocellular carcinoma antigen gene 520). CHP2 protein shares high homology with

* This work was supported by Grant-in-aid for Priority Areas 13142210 and Grant-in-aid for Scientific Research 14580664 from the Ministry of Education, Science, and Culture of Japan and by the promotion of Fundamental Studies in Health Science of the Organization for Pharmaceutical Safety and Research of Japan. The costs of publication of this article were defrayed in part by the payment of page charges. This article must therefore be hereby marked "*advertisement*" in accordance with 18 U.S.C. Section 1734 solely to indicate this fact.

The amino acid sequence of this protein can be accessed through NCBI Protein Database under NCBI accession number NM_022097.

The nucleotide sequence(s) reported in this paper has been submitted to the GenBank™/EBI Data Bank with accession number(s) AF146019.

‡ Supported by a Japan Society for the Promotion of Science Postdoctoral Fellowship.

§ To whom correspondence should be addressed. Tel.: 81-6-6833-5012; Fax: 81-6-6872-7485; E-mail: wak@ri.ncvc.go.jp.

[1] The abbreviations used are: NHE, Na^+/H^+ exchanger; CHP, calcineurin B homologous protein; GFP, green fluorescent protein; MBP, maltose-binding protein; pH_i, intracellular pH; BCECF-AM, 2′,7′-bis-(2-carboxyethyl)-5(6)-carboxyfluorescein acetoxymethyl ester; EIPA, 5-(*N*-ethyl-*N*-isopropyl)amiloride; RT, reverse transcription.

CHP1 (61% amino acid identity). This prompted us to study functional differences between the two CHP isoforms, because such investigation would provide an important clue as to the role of CHP in the NHE1 regulation.

In this study, we found that cells co-expressing NHE1 and CHP2 but not cells co-expressing NHE1 and CHP1 maintain high pH_i through the activation of NHE1 even in the absence of serum. In addition, such cells remain viable even after serum starvation over 1 week. We conclude that the interaction of NHE1 with CHP2 but not with CHP1 leads to serum-independent permanent activation of NHE1, which is a well documented property found in malignantly transformed cells.

EXPERIMENTAL PROCEDURES

Antibodies and Other Materials—Polyclonal antibodies against NHE1 (RP-cd) and CHP1 (designated anti-CHP) were described previously (6). Anti-CHP antibody, which was produced by immunizing rabbit with glutathione *S*-transferase fusion protein containing a full-length CHP1, recognized both CHP1 and CHP2. To produce isoform-specific CHP antibodies (anti-CHP1 and anti-CHP2), we immunized rabbits with synthetic peptides (^{96}NEKSKDVNGP^{105} for human CHP1 and ^{96}EDTETQDPKKP^{106}for human CHP2, see Fig. 1*A*) conjugated with keyhole limpet hemocyanin. Immunoblot analysis using recombinant CHP1 or CHP2 proteins revealed that anti-CHP2 exclusively recognized CHP2, whereas anti-CHP1 recognized CHP1 and to a lesser extent CHP2. Various human malignantly transformed cell lines, *i.e.* hepatoma, colon adenocarcinoma, cervical carcinoma, and lymphocytic leukemia cells, were obtained from the Japan Health Sciences Foundation. Human fibroblasts were obtained from a skin biopsy sample. The amiloride derivative EIPA was a gift from New Drug Research Laboratories of Kanebo, Ltd. (Osaka, Japan). ^{22}NaCl and ^{14}C-benzoic acid were purchased from PerkinElmer Life Sciences. All other chemicals were of the highest purity available.

Cells Culture and Stable Expression—The Na^+/H^+ exchanger-deficient cell line (PS120) (29), the corresponding transfectants, human skin fibroblasts, and most of cancer cell lines were maintained in Dulbecco's modified Eagle's medium (Invitrogen) containing 25 mM $NaHCO_3$ and supplemented with 7.5–10% (v/v) fetal calf serum, penicillin (50 units/ml), and streptomycin (50 μg/ml). Leukemia cells were maintained in RPMI 1640 medium containing 10% serum. Cells were maintained at 37 °C in presence of 5% CO_2. PS120 cells (5×10^5 cells/100-mm dish) were transfected with each plasmid construct (20 μg) by the calcium phosphate co-precipitation technique. Cell populations stably expressing mutant NHE1 were selected by "H^+-killing" procedure as described previously (30). Cells stably overexpressing CHP1 or CHP2 were first selected with G418, and then single colonies were isolated by checking protein expression with immunoblot while cells expressing GFP-tagged CHP were selected with the aid of GFP fluorescence.

Construction of Expression Vectors—cDNAs of CHP1 and CHP2 were isolated by means of RT-PCR using cDNAs prepared from human blood or commercially available cDNAs (human MTC™ panel I, Clontech) as a template. A cDNA for NHE6 was kindly provided by Drs. M. Sakaguchi and K. Mihara (Kyushu University, Fukuoka, Japan). All the constructs were produced by means of the PCR-based strategy. GFP-untagged and tagged CHPs were constructed by inserting PCR fragments with and without a stop codon (TAA) into pEGFP-N1 (Clontech), respectively. Plasmids carrying cDNAs for human NHE1, rat NHE2, or NHE3 and their variants were all cloned into mammalian expression vector pECE. For construction of oocyte expression vectors, cDNAs for CHPs and NHEs were inserted into the modified pBluescript II containing poly(T^+). The cRNAs were synthesized with the mCAP™ RNA capping kit (Stratagene) using linearized DNA templates. Inserted DNA fragments were confirmed by sequencing plasmids with a DNA sequencer model 3100 (ABI) to ensure the fidelity of construction.

Purification of Recombinant Proteins and Pull-down Assay—For the production of recombinant CHP2 proteins, the DNA fragment was designed to contain six His residues and cloned into a bacterial expression vector pET11a (Stratagene), which was then expressed in *Escherichia coli* (BL21). For the production of MBP fusion proteins for human NHE1 or NHE6, the DNA fragments (amino acids 503–815 of NHE1 or amino acids 500–669 of NHE6) were incorporated into pMAL-c (New England Biolabs), and plasmids were incorporated into *E. coli* (HB101). Proteins were subsequently purified by using ProBond™ (Invitrogen) or amylose (New England Biolabs) resin column according to the manufacturer's protocol. For pull-down assay, CHP2 protein was incubated for 30 min at 4 °C with 30 μl of amylose resin pretreated with MBP-NHE fusion protein in Tris-buffered saline (150 mM NaCl and 10 mM Tris-Cl, pH 7.4). After washing five times, the protein was eluted from amylose resin with 50 mM maltose, electrophoresed, and then visualized by Coomassie Brilliant Blue staining.

Immunoprecipitation and Immunoblotting—Immunoprecipitation and immunoblotting were performed essentially as described previously (31). Cells were solubilized with 1% Triton X-100 containing 150 mM NaCl, 10 mM Hepes-Tris, pH 7.4, and protease inhibitors, and cell lysate was incubated with respective antibodies and protein A-Sepharose. After centrifugation, precipitated materials were separated on 7.5 or 12% polyacrylamide gels and transferred to Immobilon membranes (Millipore). After blocking, incubation with antibodies, and washing, protein signals were visualized with enhanced chemiluminescence (Amersham Biosciences).

Measurement of ^{22}Na Uptake—$^{22}Na^+$ uptake activity was measured by the potassium$^+$/nigericin pH_i clamp method (32). Serum-supplemented or depleted cells in 24-well dishes were preincubated for 30 min at 37 °C in Na^+-free choline chloride/potassium chloride medium containing 20 mM Hepes-Tris, pH 7.4, 1.2–140 mM KCl, 2 mM $CaCl_2$, 1 mM $MgCl_2$, 5 mM glucose, and 5 μM nigericin. $^{22}Na^+$ uptake was started by adding the same choline chloride/potassium chloride solution containing ^{22}NaCl (1 μCi/ml) (final concentration, 1 mM), 1 mM ouabain, and 100 μM bumetanide. In some wells, the uptake solution contained 0.1 mM EIPA. After 1 min, cells were rapidly washed four times with ice-cold phosphate-buffered saline to terminate $^{22}Na^+$ uptake. The pH_i was calculated from the imposed [K^+] gradient by assuming intracellular K^+ concentration of 120 mM.

Measurement of pH_i—Cells were grown on Cellgen (Koken Ltd.) coated plastic coverslips, and a group of cells were serum-depleted for 24 h. Cells were loaded with 1 μM BCECF for 10 min in the buffer (140 mM NaCl, 5 mM KCl, 1.8 mM $CaCl_2$, 1 mM $MgCl_2$, and 10 mM Tris-Cl, pH 7.4), washed, and immediately mounted on coverslips. As indicated, the medium contained additionally 10% serum and/or 25 mM $NaHCO_3$. BCECF fluorescence was measured at a constant emission wavelength (550 nm) by alternately exciting the dye at 440 and 490 nm on fluorescence spectrophotometer (Spex). pH_i was calibrated in nigericin (25 μM) containing high K^+ buffer (130 mM KCl, 2 mM $CaCl_2$, 1 mM $MgCl_2$, and 30 mM Hepes-Cl, adjusted usually to pHs 6.8, 7.0, 7.2, 7.4, and 7.6). As indicated, this calibration solution additionally contained 10% serum and/or 25 mM $NaHCO_3$. Change in pH_i was also measured by the [^{14}C]benzoic acid-equilibration method (Fig. 8*B*) (30). For this measurement, serum-depleted cells were preincubated for 30 min in bicarbonate-free Hepes-buffered Dulbecco's modified Eagle's medium, pH 7.0, and then incubated in the same medium containing [^{14}C]benzoic acid (1 μCi/ml) for 10 min at 37 °C. After washing four times with ice-cold phosphate-buffered saline, ^{14}C radioactivity taken up by cells was measured. Change in pH_i was calculated as described previously (30).

Oocyte Experiment—Xenopus oocytes were stripped and defolliculated enzymatically with 1 mg/ml collagenase in Ca^{2+}-free ND96 solution (96 mM NaCl, 2 mM KCl, 1 mM $MgCl_2$, and 5 mM Hepes-NaOH, pH 7.5) for 30 min at room temperature. Defolliculated oocytes were injected with 50 nl of cRNA (50 ng) or DEPC-treated H_2O using a 10-μl micropipette (Drummond Scientific Co.). Injected oocytes were kept for 3 days at 18 °C in 0.5× L-15 solution (1:1 dilution of Leibovits L-15 medium (Invitrogen) in filter-sterilized 50 mM Hepes-NaOH, pH 7.5) containing 50 units/ml nystatin (Invitrogen) and 0.1 mg/ml gentamicin (Invitrogen). Oocytes were preincubated for 1 h in NH_4Cl medium (80 mM NH_4Cl, 1 mM $CaCl_2$, 1 mM $MgCl_2$, and 10 mM Hepes-Tris, pH 7.4), washed twice with choline-chloride medium (80 mM choline-chloride, 1 mM $CaCl_2$, 1 mM $MgCl_2$, and 10 mM Hepes-Tris, pH 7.4), and then incubated for 15 min in the same medium additionally containing 1 mM ^{22}NaCl (10 μCi/ml), 1 mM ouabain, and 0 or 0.1 mM EIPA. Oocytes were washed six times with ice-cold non-radioactive choline-chloride medium, and then $^{22}Na^+$ radioactivity was measured.

RESULTS

Human CHP2 protein has a primary sequence highly homologous to those of human CHP1 (NCBI protein accession number Q99653, 61% identity), mouse CHP1 (NCBI protein accession number Q62877, 60% identity), and mouse CHP2 (NCBI protein accession number Q9D869, 80% identity) (Fig. 1*A*). Similar to CHP1, CHP2 contains an N-terminal myristoylation site (Gly-2) as well as four EF-hand Ca^{2+} binding motifs of which two ancestral sites may not bind Ca^{2+} because of the

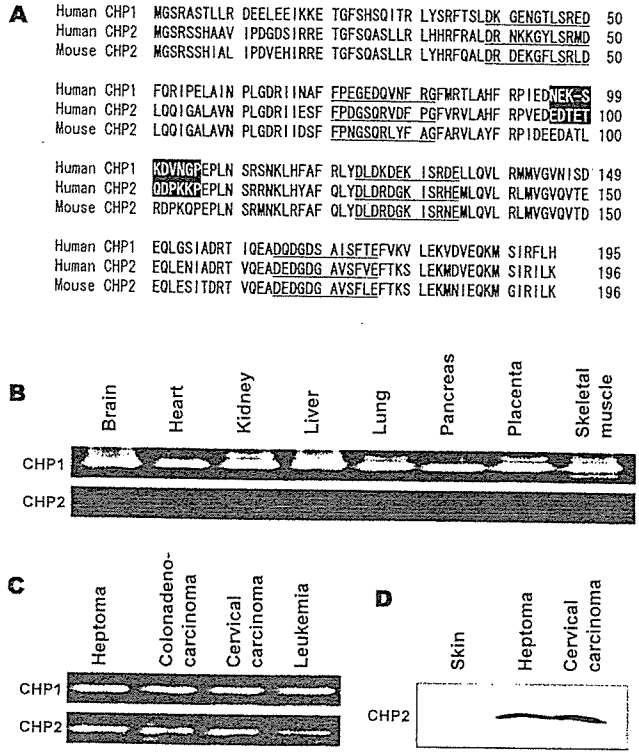

FIG. 1. **Sequence alignment and expression pattern of CHP isoforms.** *A*, amino acid sequences of human CHPs 1 and 2 and mouse CHP2 were aligned. Identical residues were *highlighted*. Four EF-hand Ca^{2+} binding motifs were *underlined* of which N-terminal two ancestral sites do not have a typical EF-hand sequence and thus may not bind Ca^{2+}. Synthetic peptide sequences used for the production of antibodies were marked by a *black box*. *B* and *C*, expression patterns of CHP1 and CHP2 were analyzed by RT-PCR. PCR reactions were performed using sets of primers 5′-tctcgggcctccacgttactgcgggacg-3′ and 5′-ATACTAGACCGCAAGAA CAG-3′ for CHP1 and 5′-CCACGCCTCTCCGGCGGGAGG-3′ and 5′-ATGGGGGCTTTGGA TGAATTC-3′ for CHP2 on templates of cDNA (1 ng) from normal tissues (human MTC panel I) or from malignantly transformed cells as indicated. After 35 cycles of PCR amplification, PCR products were analyzed on a 1% agarose gel. *D*, proteins (50 μg each) prepared from human skin fibroblasts and hepatoma and cervical carcinoma cells were subjected to immunoblot analysis with anti-CHP2 antibody.

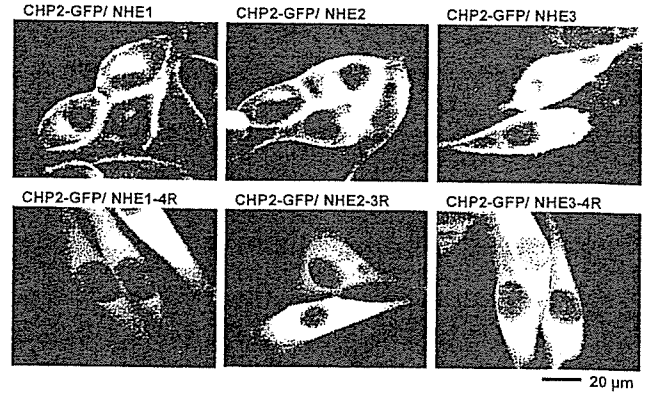

FIG. 2. **Subcellular localization of GFP-tagged CHP2.** CHP2-GFP was expressed in PS120 cells stably expressing indicated NHE variants. Enriched cell populations expressing CHP2-GFP were placed in serum-free Dulbecco's modified Eagle's medium without phenol red. Images were taken under a fluorescent microscope equipped with a CoolSNAP imaging system (RS Photometrics). In NHE1–4R, NHE2–3R, or NHE3–4R, three or four hydrophobic residues Phe^{526}, Leu^{527}, Leu^{530}, and Leu^{531} of human NHE1; Phe^{507}, Phe^{508}, and Val^{511} of rat NHE2; or Ala^{480}, Phe^{481}, Ile^{484}, and Leu^{485} of rat NHE3 were replaced by arginine residues. These mutations were reported to disrupt interaction with CHP1 (6).

substitution of critical acidic residues (Fig. 1*A*). We compared the expressions of CHP1 and CHP2 by RT-PCR using a cDNA panel from normal human tissues, *i.e.* brain, heart, kidney, liver, lung, pancreas, placenta, and skeletal muscle (human MTC™ panel I). PCR bands for CHP1 were detected in all of the human tissues tested (Fig. 1*B*). However, PCR bands for CHP2 were not detected in these tissues even after 35 cycles of PCR amplification (Fig. 1*B*). Consistent with these observations, we failed to detect CHP2 message in normal human tissues including brain, heart, skeletal muscle, colon, thymus, spleen, kidney, liver, small intestine, placenta, lung, and peripheral blood leukocyte by Northern blot analysis in which commercially available poly(A^+) RNA Northern blot (human 12-line MTN™ blot, Clontech) were hybridized with the ^{32}P-labeled full-length CHP2 probe under high stringency conditions (data not shown). In contrast to normal tissues, on the other hand, RT-PCR readily detected CHP2 as well as CHP1 in several malignantly transformed cells (Fig. 1*C*). The CHP2 expression in some cancer cells was also confirmed by immunoblot analysis (Fig. 1*D*). Taken together, these data suggest that CHP2 is expressed in malignantly transformed cells although rarely expressed in normal tissues or cells.

We previously showed that CHP1 binds to specific juxtamembrane regions (amino acids 510–530 in case of NHE1) of the cytoplasmic domains of NHEs 1–4 (6). CHP1 is also likely to bind to a corresponding region in NHE5 because of the high sequence homology of the relevant regions. We examined whether CHP2 binds to these CHP1-binding regions in NHEs 1–3 by observing subcellular localization of GFP-tagged CHP. In the exchanger-deficient PS120 cells, GFP-tagged CHP2 was uniformly distributed in the cytosol (data not shown). In contrast, in cells expressing NHE 1, 2, or 3, a part of CHP2-GFP was localized in the plasma membrane (Fig. 2). However, plasma membrane localization of CHP2-GFP was not detected in cells expressing mutant exchangers NHE1–4R, NHE2–3R, or NHE3–4R, which do not bind CHP1 (Fig. 2) (6), indicating that CHP2 also binds to CHP1-binding regions in NHEs 1–3.

Interaction of CHP2 with NHE1 was also confirmed by pull-down assay using a MBP fusion protein containing the cytoplasmic domain (aa503–815) of NHE1 (Fig. 3*A*). As a negative control, we showed that CHP2 does not bind to a MBP fusion protein containing the cytoplasmic domain (aa500–669) of NHE6 (Fig. 3*B*). These data suggest that CHP2 directly interacts with the juxtamembrane CHP1-binding site in the plasma membrane-type exchangers. To examine the relative binding efficiency of CHP1 *versus* CHP2, we carried out pull-down assay using MBP-NHE1 fusion proteins in the presence of a constant amount of CHP2 and different amounts of CHP1. As shown in Fig. 3*C*, *lower panel*, the amount of CHP2 protein recovered by pull down decreased with increasing amounts of CHP1 by competitive interaction for the common binding site in NHE1. When 250 μg of CHP1 and 50 μg of CHP2 were present, almost equal amounts of CHP1 and 2 were recovered (Fig. 3*C*), suggesting that CHP2 binds to NHE1 more strongly (~5-fold) than does CHP1.

We used the oocyte expression system to examine the role of CHP2 in the exchange activity. As shown in Fig. 4, the injection of cRNA for NHE1 or NHE3 significantly enhanced exchange activity in oocytes. Co-injection of cRNA for CHP1 or CHP2 together with cRNA for NHE1 or NHE3 further enhanced the exchange activity. The data suggest that CHP1 and CHP2 have the ability to increase exchange activities of NHE1 and NHE3 to a similar extent.

To observe the functional difference between CHP1 and CHP2, we produced stable cell clones overexpressing CHP1 or CHP2. Immunoblot analysis revealed that PS120 cells express

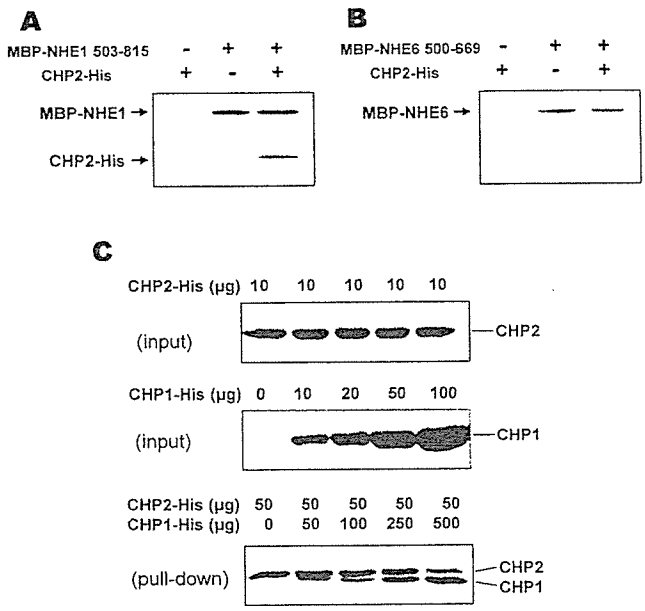

FIG. 3. **Pull-down assay for CHP-NHE interaction.** *A* and *B*, 150 μg of CHP2-His protein was mixed with 30 μl of amylose resin pretreated with 200 μg of MBP-NHE1 or MBP-NHE6 fusion protein, respectively, and incubated for 60 min. After resins were washed, proteins were eluted with 50 mM maltose, electrophoresed, and visualized by Coomassie Brilliant Blue staining. *C*, 50 μg of CHP2-His protein and different amounts of CHP1-His protein were mixed with 30 μl of amylose resin pretreated with 100 μg of MBP-NHE1 fusion protein, incubated for 60 min, eluted, and analyzed by electrophoresis (*bottom panel*). Protein inputs were also shown for reference (*upper* and *middle panels*).

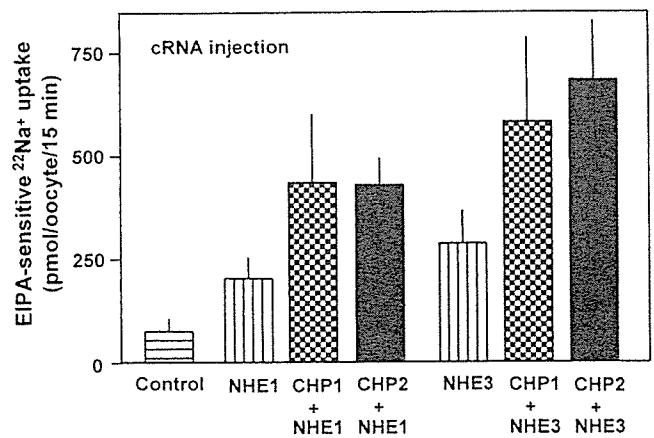

FIG. 4. **Oocyte experiment.** Three days after injection of cRNA into *Xenopus* oocytes, $^{22}Na^+$ uptake was measured in the presence or absence of 0.1 mM EIPA as described under "Experimental Procedures." Data are means ± S.D. of data from 30 oocytes.

a relatively high level of endogenous CHP1 and a very low level of endogenous CHP2 as compared with the respective proteins overexpressed in the same cells (Fig. 5). Anti-CHP1 immunoprecipitated NHE1 protein from cells co-expressing CHP1/NHE1 but not from cells co-expressing CHP2/NHE1, whereas anti-CHP2 immunoprecipitated NHE1 protein from cells co-expressing CHP2/NHE1 but not from cells co-expressing CHP1/NHE1 (Fig. 5). These antibodies immunoprecipitated much lower levels of NHE1 protein from NHE1 transfectants not expressing exogenous CHP1 or CHP2 (Fig. 5), consistent with the above finding that PS120 cells express endogenous CHP1 and CHP2. The NHE1 protein was not detected in the immunoprecipitated material obtained with anti-CHP2 from

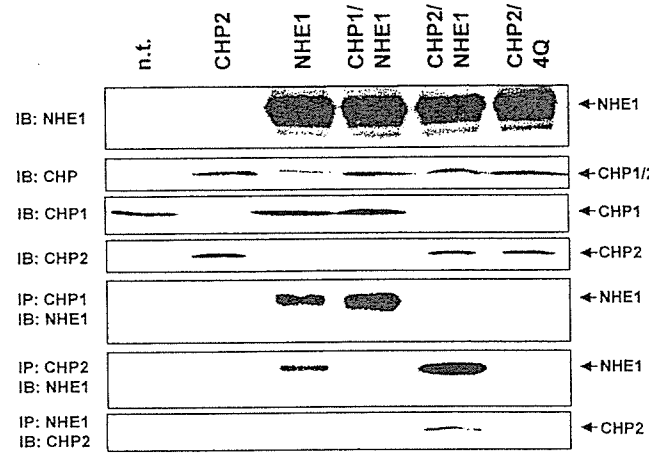

FIG. 5. **Co-immunoprecipitation analysis of CHP/NHE1 interaction.** CHPs and NHE1 variants expressed stably in PS120 cells are shown above the *panels*, whereas antibodies used are shown on the *left side* of each *panel*. In 4Q, four hydrophobic residues, Phe^{526}, Leu^{527}, Leu^{530}, and Leu^{531} of NHE1, were replaced by four glutamine residues. In the experiments for the *top four panels*, 20-μg proteins from total cell homogenate were analyzed by immunoblotting (*IB*). In the experiments for the *last three panels*, cell lysates were subjected to immunoprecipitation (*IP*) with indicated antibodies and then analyzed by immunoblotting as described under "Experimental Procedures." *n.t.*, non-transfected cells.

cells not expressing NHE1 (Fig. 5, *n.t.* or *CHP2*) or cells expressing a CHP-binding-defective NHE1 (Fig. 5, *4Q*). These data suggest that exogenous CHP1 or CHP2 replaces endogenous CHP bound to NHE1 protein.

We examined the effect of 24-h serum depletion on exchange activity in cells co-expressing CHP1/NHE1 or CHP2/NHE1 measured at different pH_i values. Both groups of cells exhibited high $^{22}Na^+$ uptake activity (50–60 nmol/mg/min) at low pH_i (5.6), independent of serum depletion (Fig. 6*A*). In CHP1/NHE1 cells, exchange activity at a neutral pH_i (6.8–7.2) was significantly lower with serum depletion than without serum depletion (Fig. 6, *B–D*). In sharp contrast, prior treatment with or without serum did not affect exchange activity significantly in CHP2/NHE1 cells at all pH_i values tested (Fig. 6, *B–D*). Consistent with $^{22}Na^+$ uptake, the resting pH_i in CHP2/NHE1 cells was significantly elevated (7.4–7.5) in the absence (Fig. 7*A*) or presence (Fig. 7*B*) of bicarbonate regardless of prior treatment with or without serum, whereas pH_i was significantly lower in CHP1/NHE1 cells subjected to serum deprivation. Thus, NHE1 was constitutively activated in cells expressing CHP2/NHE1. Of note, long serum depletion significantly reduces pH_i in CHP2 transfectants not expressing NHE1 (Fig. 7) or in cells co-expressing the CHP-binding-defective NHE1 mutant 4Q and CHP2 (data not shown). Such an effect was also observed in non-transfected PS120 cells (data not shown), suggesting that relatively long serum depletion may affect other pH_i-regulating systems.

We next examined the acute effect of serum addition on pH_i of cells that had been maintained for 24 h under serum depletion. Serum induced a relatively large cytoplasmic alkalinization in CHP1/NHE1 cells as measured by BCECF fluorescence (Fig. 8*A*) or ^{14}C-benzoic acid equilibration method (Fig. 8*B*). Cytoplasmic alkalinization occurred similarly in NHE1 cells or in CHP1/NHE1 cells (Fig. 8*B*). In contrast, serum addition caused a minimum alkalinization in CHP2/NHE1 cells. Alkalinization was not observed in CHP2 transfectants not expressing NHE1 or in CHP2 transfectants expressing 4Q (Fig. 8, *A* and *B*). These results confirmed that NHE1 was already activated in CHP2/NHE1 transfectants maintained in the absence of serum.

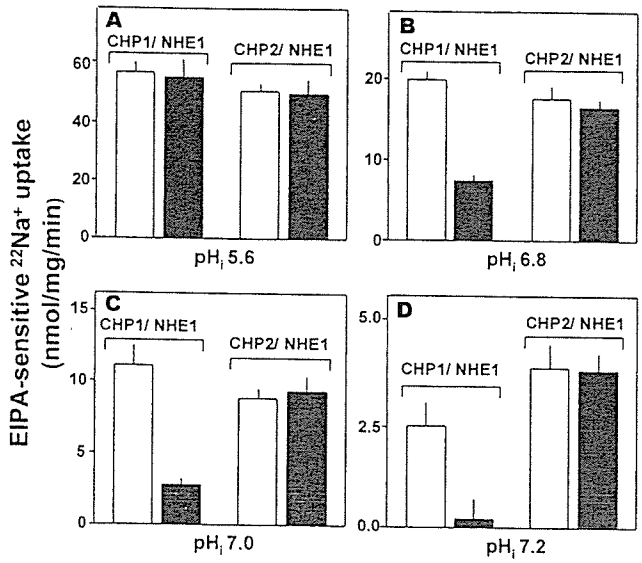

FIG. 6. **The effect of serum depletion on $^{22}Na^+$ uptake activity.** PS120 cells stably co-expressing CHP1/NHE1 or CHP2/NHE1 grown in 24-wells were serum-depleted for 24 h. The pH_i values of serum-supplemented (*open bars*) or serum-depleted cells (*closed bars*) were clamped at 5.6, 6.8, 7.0, or 7.2 by incubating cells in the solutions containing nigericin and the appropriate concentrations of KCl, and then EIPA-sensitive $^{22}Na^+$ uptake was measured as described under "Experimental Procedures." Data are means ± S.D. (n = 9).

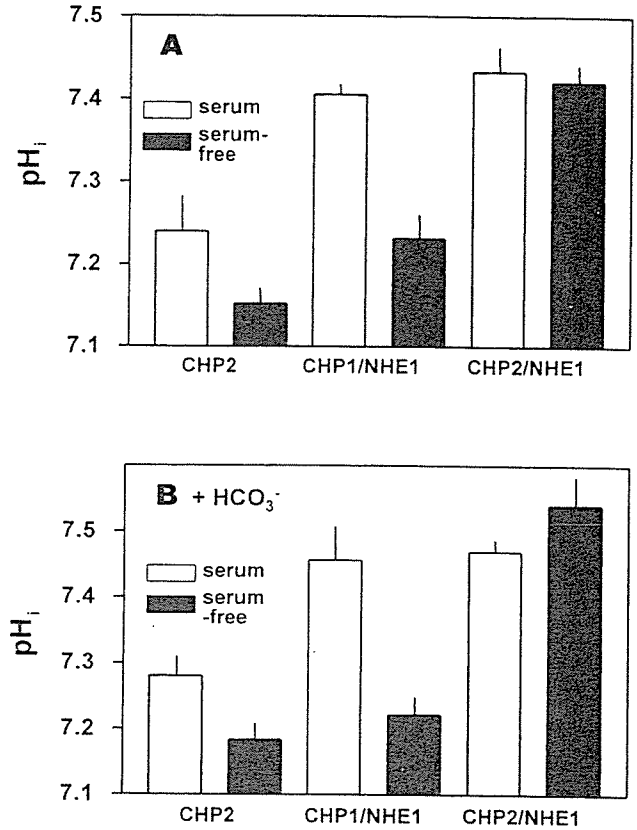

FIG. 7. **The effect of serum depletion on the resting pH_i.** The resting pH_i of PS120 cells expressing CHP2, CHP1/NHE1, or CHP2/NHE1, which were maintained for 24 h in the presence (*open bars*) or absence (*closed bars*) of serum, was measured in the absence (*A*) or presence (*B*) of 25 mM $NaHCO_3$ by monitoring BCECF fluorescence as described under "Experimental Procedures." Data are means ± S.D. (n = 9).

Intracellular pH has been reported to influence both cell growth (4) and cell viability (20–23, 33–36). Indeed, cell number increased efficiently in the presence of serum upon expression of NHE1 regardless of the type of CHP isoform co-expressed, whereas cells expressing 4Q grew relatively slowly (Fig. 9*A*). Despite this apparently similar role of CHP1 and CHP2 in cell growth, the ability to maintain cell viability under serum starvation was dramatically different between cells expressing NHE1/CHP1 and NHE1/CHP2 (Fig. 9*B*). We evaluated cell viability by counting the number of cells remained attached to dishes during serum starvation. These cells excluded trypan blue and were able to restart growth upon re-addition of serum. Cells expressing CHP2/NHE1 were significantly more resistant to serum starvation ($t_{1/2}$ = ~14 days) than cells expressing CHP1/NHE1 ($t_{1/2}$ = ~4 days). Surprisingly, 60% of cells expressing CHP2/NHE1 were still viable 10 days after serum starvation when all CHP1/NHE1 cells lost viability (Fig. 9*B*). The high viability of CHP2/NHE1 cells required enhanced NHE1 activity but not the expression of CHP2 itself, because both CHP2 or CHP2/4Q cells were very sensitive to serum starvation ($t_{1/2}$ = ~2 days) (Fig. 9*B*) and because EIPA markedly accelerated the loss of viability in CHP2/NHE1 cells (Fig. 9*C*). These data suggest that the high viability of CHP2/NHE1 cells may be the result of high pH_i caused by high Na^+/H^+ activity achieved in these serum-starved cells.

DISCUSSION

In this study, we characterized the function of CHP2 that shares a high sequence homology with CHP1. We previously reported that CHP1 serves as an essential cofactor, supporting the physiological activity of plasma membrane-type Na^+/H^+ exchangers (6). CHP2 exerts similar effects. (i) GFP-tagged CHP2 co-localized with NHEs 1–3 but not with CHP1-binding-defective mutants NHE1–4R, NHE2–3R, or NHE3–4R in the plasma membrane. (ii) Recombinant CHP2 was bound to a MBP fusion protein containing the NHE1 cytoplasmic domain but not the fusion protein containing NHE6 cytoplasmic domain. (iii) CHP2 enhanced exchange activities of NHE1 and NHE3 when co-expressed with them in oocytes. (iv) The V_{max} of CHP2/NHE1 was comparable with that of CHP1/NHE1, whereas CHP2/4Q cells exhibited a very low exchange activity (<10%) compared with CHP2/NHE1.

Intriguingly, CHP1/NHE1 and CHP2/NHE1 cells responded differently to serum depletion, although they exhibited a similar high exchange activity when maintained in serum. In the absence of serum, CHP2/NHE1 exhibited a higher steady-state pH_i and higher exchange activity in the neutral pH_i range as compared with CHP1/NHE1. Thus, NHE1 becomes activated with bound CHP2 independent of serum. We observed that steady-state levels of pH_i in CHP1/NHE1 and CHP2/NHE1 cells maintained for 24 h in serum-supplemented or serum-depleted medium were not affected by the presence or absence of bicarbonate. In contrast, the presence of bicarbonate influenced the response of CHP1/NHE1 cells to a short incubation (10–20 min) with serum. The pH_i of CHP1/NHE1 was elevated in response to acute exposure to serum in the absence of bicarbonate (Fig. 8), but this did not happen in the presence of bicarbonate (data not shown). Such an inhibitory effect of bicarbonate on pH_i may be because of activation of the anion exchanger. At present, however, it is not clear why bicarbonate did not exhibit an inhibitory influence on pH_i in CHP1/NHE1 and CHP2/NHE1 cells chronically exposed to serum (Fig. 7).

We found that CHP2/NHE1 cells are highly viable even under a long term serum starvation. Ubiquitous CHP1 was previously suggested to be involved in various cell functions, such as inhibition of calcineurin activity (37), vesicular transport of proteins (38), interaction with microtubules (39), and interaction with a death-associated protein kinase-related

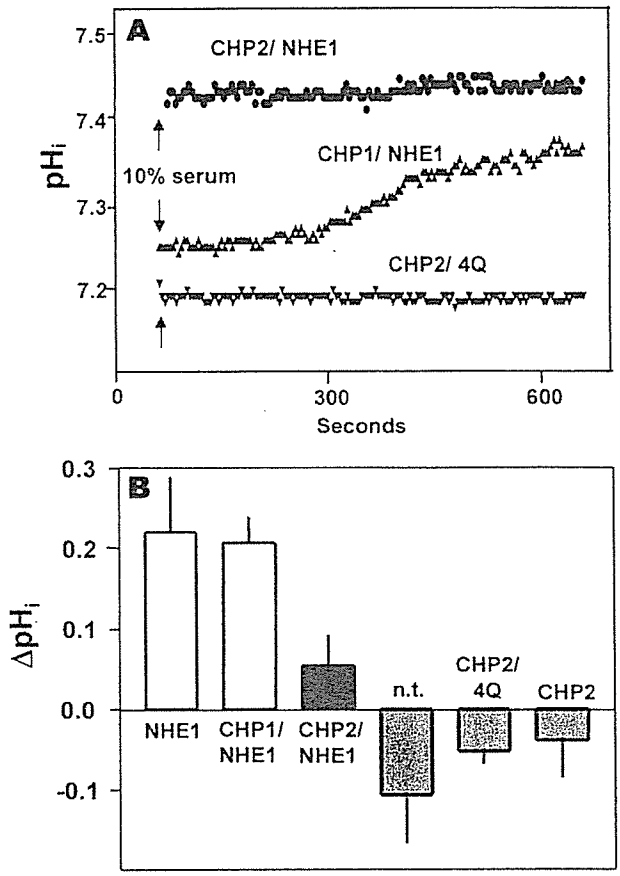

FIG. 8. **Serum-induced acute change in pH$_i$ of cells expressing CHP1 or CHP2.** *A*, serum-depleted cells were loaded with 1 μM BCECF-AM, washed, and set in fluorescent spectrophotometer. At the time indicated by an *arrow*, 10% dialyzed serum was added. Change in BCECF fluorescence was measured as described under "Experimental Procedures." *B*, change in pH$_i$ was measured by ^{14}C-benzoic acid equilibration method as described under "Experimental Procedures." Change in pH$_i$ was measured 10 min after the addition of 10% dialyzed serum. Data are means ± S.D. (n = 3). *n.t.*, non-transfected.

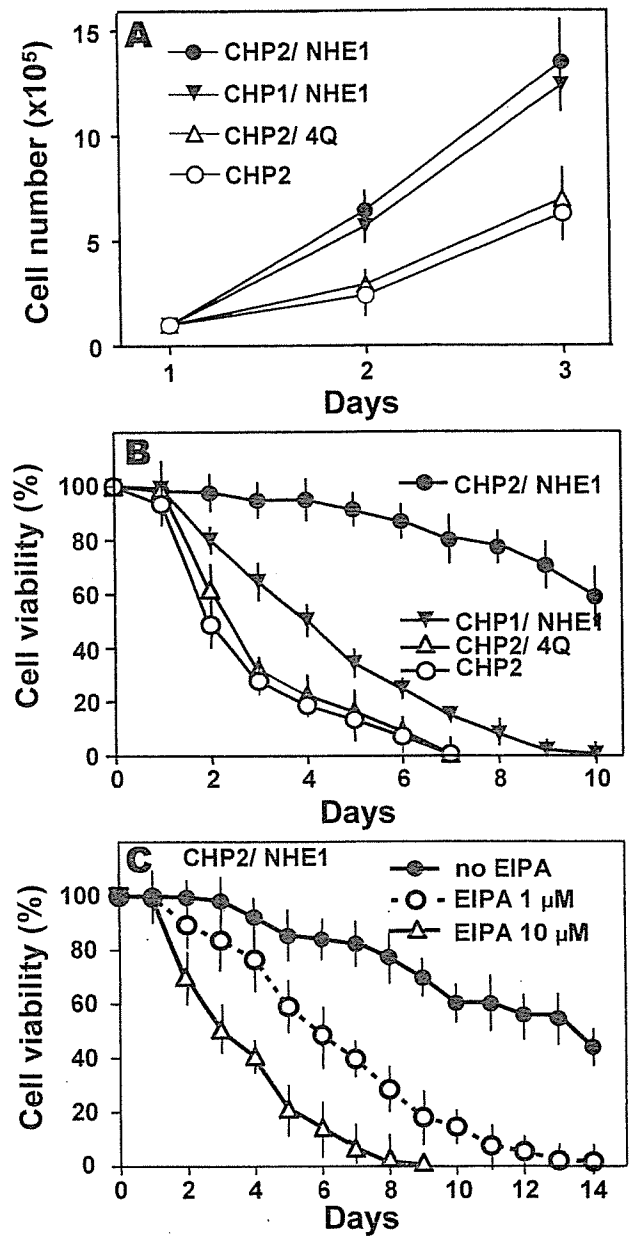

FIG. 9. **Effect of expression of CHP1 or CHP2 on cell growth and cell viability under serum starvation.** *A*, growth rate of various transfected cells was measured in the presence of 7.5% serum. At the indicated time, cells were trypsinized and counted by hemocytometer. *B* and *C*, cell viability under serum starvation. The same numbers of cells were seeded on 60-mm dishes, and 1 day later, serum was removed. *C*, in some dishes, the medium contained 1 or 10 μM EIPA. We counted the number of cells that remained attached in four 5 × 5-mm square areas/each dish. We counted the cell numbers in the same areas throughout experiments and plotted them in the figure. Three dishes were used for respective transfectants. Data are means ± S.D. (n = 12).

apoptosis-inducing protein kinase 2 (DRAK2) (40). Although we do not know whether CHP2 is also involved in these cellular functions, they may not be relevant to the observed effects of CHP2 because the functions of CHP1/NHE1 and CHP2/NHE1 were compared in this study. However, we cannot rule out a possibility that cellular functions specific to CHP2 may be involved in the observed CHP2 effect. At any rate, it is probable that high viability of CHP2/NHE1 cells results from maintenance of high pH$_i$ through serum-independent activation of NHE1, because cells overexpressing CHP2 were sensitive to serum starvation when active NHE1 was not expressed or when EIPA was present in the medium. Factors such as ultraviolet light, Fas ligand, somatostatin, and IgM are known to induce cell acidification, which precedes apoptotic cell death in various cell types such as Jurkat cells (33), HL-60 leukemia cells (34, 36), human B lymphomas (21, 22), and human breast cancer cells (20, 35). Our data also suggest that pH$_i$ is an important determinant for serum deprivation-induced cell death.

We found that relatively high levels of CHP2 mRNA were detected in several types of malignantly transformed cells but not in normal tissues or cells. This is consistent with previous findings that CHP2 expression was detected in liver carcinoma cells (GenBank™ nucleotide accession number AF146019) and colon tumor metastatic cells (GenBank™ nucleotide accession number EST370271). It has been well documented that malignantly transformed cells maintain abnormally high pH$_i$. For example, microinjection of *ras* p21 protein (25) and stable transfection of Ha-*ras* oncogene (26, 27) or E7 oncogene of papillomavirus type 16 (28) resulted in a marked increase in the steady-state pH$_i$ in NIH-3T3 cells through the activation of NHE1. Moreover, high pH$_i$ because of activation of NHE1 has been observed in various malignantly transformed cells, such as human leukemic (21), human malignant glioma (41), and human breast cancer cells (42). Interestingly, in this latter study (42), pH$_i$ was shown to be higher under serum-deprived

rather than under serum-supplemented conditions. All of these studies suggest that NHE1 becomes permanently activated in many malignantly transformed cells, although the molecular mechanism for such a phenomenon remains unclear. The properties of NHE1 in these transformed cells are similar to those of CHP2/NHE1 observed here. CHP2 appears to be almost exclusively expressed in these transformed cells. In addition, NHE1 interacts more strongly with CHP2 than with CHP1. Therefore, we propose that the activation of NHE1 by bound CHP2 may be a key mechanism for the maintenance of serum-independent high pH_i in these abnormal cells.

At present, we do not know how NHE1 is activated by CHP2. A previous study (5) suggested that serum changes the phosphorylation state of CHP1. Although it is not clear whether phosphorylation of CHP1 is a key event in the growth factor-induced activation of NHE1 in normal cells, the difference in the phosphorylation status could be one possible mechanism to explain the observed difference in the mode of serum-dependent regulation of NHE1 by CHP1 or CHP2. Indeed, there are several potential phosphorylation sites that differ between CHP1 and CHP2. For example, potential phosphorylation sites for protein kinase C (Ser^{112}) or calmodulin-dependent protein kinase II (Thr^{7}, Ser^{33}, and Ser^{37}) in CHP1 are not conserved in CHP2. Alternatively, these CHP isoforms may interact with different proteins that mediate different signals from serum to NHE1·CHP complex. Further studies including analyses with chimeric or mutated CHPs and determination of the crystal structure of NHE1·CHP complex are required to elucidate the molecular mechanism in the generation of the functional difference between CHP1 and CHP2.

In summary, the present data suggest that the interaction of NHE1 with CHP2 leads to serum-independent permanent activation of NHE1, which in turn results in the protection of cells from serum deprivation-induced death. A recent study (28) has reported that NHE1 inhibitor markedly retarded the development of tumor in nude mice. Our study suggests that CHP2 may be a novel important target for anticancer therapy as it appears to be almost exclusively expressed in malignantly transformed cells.

REFERENCES

1. Wakabayashi, S., Shigekawa, M., and Pouysségur, J. (1997) *Physiol. Rev.* **77,** 51–74
2. Orlowski, J., and Grinstein, S. (1997) *J. Biol. Chem.* **272,** 22373–22376
3. Counillon, L., and Pouysségur, J. (2000) *J. Biol. Chem.* **275,** 1–4
4. Grinstein, S., Rotin, D., and Mason, M. J. (1989) *Biochim. Biophys. Acta* **988,** 73–97
5. Lin, X., and Barber, D. L. (1996) *Proc. Natl. Acad. Sci. U. S. A.* **93,** 12631–12636
6. Pang, T., Su, X., Wakabayashi, S., and Shigekawa, M. (2001) *J. Biol. Chem.* **276,** 17367–17372
7. Bertrand, B., Wakabayashi, S., Ikeda, T., Pouysségur, J., and Shigekawa, M. (1994) *J. Biol. Chem.* **269,** 13703–13709
8. Wakabayashi, S., Bertrand, B., Ikeda, T., Pouysségur, J., and Shigekawa, M. (1994) *J. Biol. Chem.* **269,** 13710–13715
9. Wakabayashi, S., Ikeda, T., Noel, J., Schmitt, B., Orlowski, J., Pouysségur, J., and Shigekawa, M. (1995) *J. Biol. Chem.* **270,** 26460–26465
10. Voyno-Yasenetskaya, T., Conklin, B. R., Gilbert, R. L., Hooley, R., Bourne, H. R., and Barber, D. L. (1994) *J. Biol. Chem.* **269,** 4721–4724
11. Dhanasekaran, N., Prasad, M. V., Wadsworth, S. J., Dermott, J. M., and Van Rossum, G. (1994) *J. Biol. Chem.* **269,** 11802–11806
12. Hooley, R., Yu, C.-Y., Symons, M., and Barber, D. L. (1996) *J. Biol. Chem.* **271,** 6152–6158
13. Bianchini, L., L'Allemain, G., and Pouysségur, J. (1997) *J. Biol. Chem.* **272,** 271–279
14. Takahashi, E., Abe, J.-I., Gallis, B., Aebersold, R., Spring, D. J., Krebs, E. G., and Berk, B. C. (1999) *J. Biol. Chem.* **274,** 20206–20214
15. Lehoux, S., Abe, J. I., Florian, J. A., and Berk, B. C. (2001) *J. Biol. Chem.* **276,** 15794–15800
16. Yan, W., Nehrke, K., Choi, J., and Barber, D. L. (2001) *J. Biol. Chem.* **276,** 31349–31356
17. Aharonovitz, O., Zaun, H. C., Balla, T., York, J. D., Orlowski, J., and Grinstein, S. (2000) *J. Cell Biol.* **150,** 213–224
18. Rao, G. N., Roux, N., Sardet, C., Pouysségur, J., and Berk, B. C. (1991) *J. Biol. Chem.* **266,** 13485–13488
19. Wang, H., Singh, D., and Fliegel, L. (1997) *J. Biol. Chem.* **272,** 26545–26549
20. Thangaraju, M., Sharma, K., Liu, D., Shen, S. H., and Brikant, C. B. (1999) *Cancer Res.* **59,** 1649–1654
21. Rich, I. N., Worthington-White, D., Garden, O. A., and Musk, P. (2000) *Blood* **95,** 1427–1434
22. Marches, R., Vitetta, E. S., and Uhr, J. W. (2001) *Proc. Natl. Acad. Sci. U. S. A.* **98,** 3434–3439
23. Sailer, B. L., Barrasso, A. M., Valdez, J. G., Cobo, J. M., D'Anna, J. A., and Crissman, H. A. (1998) *Cancer Res.* **58,** 413–420
24. Gillies, R. J., Martinez-Zaguilan, R., Martinez, G. M., Serrano, R., and Perona, R. (1990) *Proc. Natl. Acad. Sci. U. S. A.* **87,** 7414–7418
25. Hagag, N., Lacal, J. C., Graber, M., Aaronson, S., and Viola, M. V. (1987) *Mol. Cell. Biol.* **7,** 1984–1988
26. Maly, K., Uberall, F., Loferer, H., Doppler, W., Oberhuber, H., Groner, B., and Grunicke, H. H. (1989) *J. Biol. Chem.* **264,** 11839–11842
27. Kaplan, D. L., and Boron, W. F. (1994) *J. Biol. Chem.* **269,** 4116–4124
28. Reshkin, S., J., Bellizzi, A., Caldeira, S., Albarani, V., Malanchi, I., Poignee, M., Alunni-Fabbroni, M., Casavola, V., and Tommasino, M. (2000) *FASEB J.* **14,** 2185–2197
29. Pouysségur, J., Sardet, C., Franchi, A., L'Allemain, G., and Paris, S. (1984) *Proc. Natl. Acad. Sci. U. S. A.* **81,** 4833–4837
30. Wakabayashi, S., Fafournoux, P., Sardet, C., and Pouysségur, J. (1992) *Proc. Natl. Acad. Sci. U. S. A.* **89,** 2424–2428
31. Wakabayashi, S., Pang, T., Su, X., and Shigekawa, M. (2000) *J. Biol. Chem.* **275,** 7942–7949
32. Ikeda, T., Schmitt, B., Pouysségur, J., Wakabayashi, S., and Shigekawa, M. (1997) *J. Biochem. (Tokyo)* **121,** 295–303
33. Gottlieb, R. A., Nordberg, J., Skowronski, E., and Babior, B. M. (1996) *Proc. Natl. Acad. Sci. U. S. A.* **93,** 654–658
34. Takasu, T., Lyons, J. C., Park, H. J., and Song, C. W. (1998) *Cancer Res.* **58,** 2504–2508
35. Thangaraju, M., Sharma, K., Leber, B., Andrews, D. W., Shen, S. H., and Brikant, C. B. (1999) *J. Biol. Chem.* **274,** 29549–29557
36. Kluza, J., Lansiaux, A., Wattez, N., Mahieu, C., Osheroff, N., and Bailly, C. (2000) *Cancer Res.* **60,** 4077–4084
37. Lin, X., Sikkink, R. A., Rusnak, F., and Barber, D. L. (1999) *J. Biol. Chem.* **274,** 36125–36131
38. Barroso, M. R., Bernd, K. K., DeWitt, N. D., Chang, A., Mills, K., and Sztul, E. S. (1996) *J. Biol. Chem.* **271,** 10183–10187
39. Timm, S., Titus, B., Bernd, K., and Barroso, M. (1999) *Mol. Biol. Cell* **10,** 3473–3488
40. Matsumoto, M., Miyake, Y., Nagita, M., Inoue, H., Shitakubo, D., Takemoto, K., Ohtsuka, C., Murakami, H., Nakamura, N., and Kanazawa, H. (2001) *J. Biochem. (Tokyo)* **130,** 217–225
41. McLean, L. A., Roscoe, J., Jorgensen, N. K., Gorin, F. A., and Cala, P. M. (2000) *Am. J. Physiol.* **278,** C676–C688
42. Reshkin, S., J., Bellizzi, A., Albarani, V., Guerra, L., Tommasino, M., Paradiso, A., and Casavola, V. (2000) *J. Biol. Chem.* **275,** 5361–5369

Future Investigations of Micro-Macro Level Cardiac Functions Using X-ray Diffraction

James Todd Pearson*, Naoto Yagi**, Mikiyasu Shirai*, Naoki Nishiura*, Munetake Kanda*, Noriyuki Tokunaga*, Hiroyuki Suga* and Hidezo Mori*

放射光を用いたX線回折手法は，これまで摘出心筋に広く応用され，収縮タンパクのphenotypeの分子的な違いが，心筋の収縮過程にどのように影響するかが明らかにされた．回折像には，2つの顕著な回折ピーク（1，0）反射と（1，1）反射があり，心筋収縮によってそれらの強度は変化した．両者の強度比は，アクチン，ミオシン間の質量移動を反映し，心筋短縮中のクロスブリッジ動態を知るための有効な指標と考えられた．最近では，強度と時間分解能の技術改良によって，マウスの生体内心臓にも応用可能となってきた．各遺伝子とその産生タンパクが容易に操作できるトランスジェニックマウスでのX線回折強度と心室圧-容積関係の実時間解析は，ミクロとマクロレベルでの心収縮機構の統合的理解を飛躍的に促進する可能性がある．特に，サルコメアを構成するミオシンやトロポニンなどの異常遺伝子を導入したマウスでの解析は，心臓の収縮力と収縮の機械的効率を解明するための重要な手掛かりを提供するであろう．

X-ray diffraction has revealed a great deal about the molecular structure changes in isolated papillary muscle during contractions, but ultimately the challenge is to use X-ray diffraction to examine how cardiovascular function is related to interactions between micro-macro levels. That is a formidable leap, which will undoubtedly only result from the progress of many research laboratories. Nevertheless, we are now at the stage of attempting X-ray diffraction measurements of whole mice and rat hearts *in vivo*. Mice in particular, will play a key role in the future of medical research using X-ray diffraction because of the ease with which new transgenic models can be generated for different cardiovascular disease states. However, establishing the fundamental relationships between cardiac performance at micro-macro levels in mice is also the greatest challenge to this field. Although highly invasive, open-chest mouse and rat models allow us to determine the capabilities of the heart, including the performance of the left and right hearts individually, and also allow us to manipulate blood flow and myocardial contractility.

* 国立循環器病センター
** 高輝度光科学研究センター

1. Synchrotron Radiation and Molecular Level Studies of Cardiac Muscle

Synchrotron radiation is the only source of X-ray radiation that is strong enough and sufficiently focused to be able to identify the organization of lattice structures at the molecular level of proteins. The lattice arrangement of the two basic contractile protein elements, myosin and actin, can be demonstrated from the diffracted spectra that result when X-ray radiation is applied to the short axis (equatorial plane) of the elongated muscle fibers (Fig. 1). The reflections at the detector form two main peaks of intensity separated by less than 0.5 degrees, identified as (1, 0) and (1, 1) respectively, that relate to the spacing

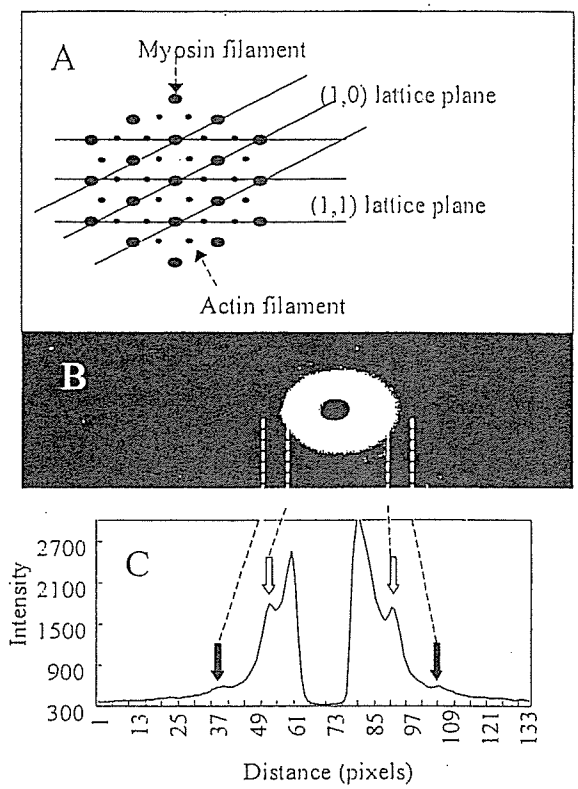

Fig. 1 A. Hexagonal lattice arrangement of thick and thin filaments of a muscle fiber in the equatorial plane showing 1, 0 (all thick filaments) and 1, 1 planes (2 thin filaments to every 1 thick filament) taken from Matsubara and Millman[12]. B. A typical equatorial scattering pattern resulting from small angle diffraction of synchrotron radiation obtained from a whole rat heart *in vivo*. C. Resultant diffraction pattern showing differences in intensity of (1, 0) and (1, 1) reflections (open and solid arrows respectively).

between lattice elements[1]. The spacing between (1, 0) peaks in the diffraction pattern is inversely proportional to the spacing between lattice planes, which has been demonstrated to correspond to sarcomere length[2-4]. Huxley and Brown[5] long ago proposed that during skeletal muscle contractions myosin filaments slide along actin filaments resulting in the shortening of muscle fibers, which was based on their results of small angle X-ray diffraction experiments. The mechanism for sliding movements between filaments within muscle fibers was attributed to cyclic attachment of the heads of myosin to actin filaments, termed crossbridges, after Ca^{2+} levels are elevated during contraction and flex, resulting in greater overlap between actin-myosin filaments, shortening of the fibers and development of tension[6]. In resting skeletal muscles the intensity of the (1, 1) reflection peak is less than that of the (1, 0) peak, but with the start of an isometric contraction the intensity of the (1, 1) peak increases relative to (1, 0) independent of filament sliding as more crossbridges bind to actin molecules[7,8]. However, the change in intensity ratio alone is not the only important parameter, as it was demonstrated early that gradual displacement of crossbridges by a slow stretch in excess of maximal isometric contraction created greater tension for the same number of crossbridge attachments, suggesting that crossbridge position also has an important influence on the tension developed[9].

Cardiac muscle differs very little from skeletal muscle in terms of filament structure, but contrasts skeletal muscle with respect to the mechanism of stimulation and flux of Ca^{2+} ions. Cross-bridge transfer from myosin to actin during cardiac contractions was first confirmed by an X-ray diffraction technique using papillary muscles *in situ* and excised from the right ventricle of canine hearts[10,11], although similar measurements were made earlier with papillary muscle in a state of rigor, with maximal crossbridge attachment[12]. A maximum of 70-71% of crossbridges were transferred to actin filaments during systole and 50-52% during diastole[10,11,13]. Increased frequency of contraction results in greater peak tension and more crossbridges being transferred during systole[14]. Thus even during diastole the number of crossbridges remaining in the vicinity of actin filaments is higher than that found in resting muscle fibers, even though no significant force is developed[13,15-17]. Early studies required thousands of isometric contractions to obtain sufficiently intense reflections, which were accumulated separately for systole and diastole (each exposure was 300-500 ms). With technological improvements in both X-ray power, image intensification and time resolution (currently 10 ms with fast CCD cameras) it is now possible to identify the time course of changes in intensity ratio of the reflections ($I_{1,0}/I_{1,1}$) for single twitch stimulations *ex vivo*, albeit at low temperatures of 27-30°C[18,19].

After those pioneering studies other researchers have investigated how mass transfer relates to muscle tension, sarcomere length and loading conditions. Fractional increase in the intensity ratio

precedes the development of normalized tension in papillary muscle under isometric contraction, although changes in both parameters peak at a similar time after stimulation[20]. The decrease in intensity ratio after the peak in tension is considerably delayed in relation to the decrease in tension. The difference in time course between crossbridge mass transfer and normalized tension is attributed to the existence of weak and strong binding states[21]. Even after the surge of cytosolic Ca^{2+} ions and the opening of the actin binding sites the crossbridges attach to actin in an initial weak binding state, but no force is developed until after a conformational change in the myosin head, leading to the power stroke from energy stored in the head from ATP hydrolysis during the previous diastole. It remains unclear whether the transition to strong binding state is a consequence of the Ca-troponin-C interaction, but a direct effect of Ca^{2+} ion on myosin ATPase is unlikely[22]. Nevertheless, troponin-C regulates the opening of actin binding sites. Current X-ray diffraction techniques are unable to distinguish between these binding states and thus, mass transfer of crossbridges appears to be incompletely synchronized with the development of tension. The exaggerated delay in the decrease of the intensity ratio suggests that myosin heads remain in close proximity to actin for some time after detachment. The extent of mass transfer that occurs during isometric contractions is inversely related to sarcomere length, in accordance with Starling's Law of the Heart. Okuyama and associates[20] also observed that even with reductions in developed tension under isotonic contractions the number of participating crossbridges is relatively unchanged in comparison to maximal isometric contraction.

The next steps toward *in vivo* investigations present both technical difficulties related to data acquisition and problems associated with appropriate surgical preparation of mice to obtain physiologically meaningful data. High body temperature (37-38°C) will initially limit the time resolution of reflection patterns *in vivo*. Most heart functions increase with temperature due to the Arrhenius effect. In contrast to typical conscious heart rates of 60 bpm in resting humans, heart rates in conscious mice vary between 450-800 bpm dependent on the level of activity[23,24]. Unlike isolated hearts, the performance of the whole heart is controlled by humoral factors and autonomic neural input. The latter and the heart itself, however, are greatly depressed under anaesthesia[23], and so the choice of anaesthesia in future experiments is important for two reasons. First, dependent on the choice of anaesthesia current sampling regimes every 10 ms will provide only 12-20 samples per cardiac cycle. However, time resolution should not be a barrier to progress for long. Second the large negative ionotropic effect of some anaesthetics can confound results if the aim is to determine a transgenic animal's contractile reserve. Until now X-ray studies of cardiac muscle fibers have been determined from papillary muscles, however, crossbridge kinetics may differ between ventricular free wall myocardia and papillary muscles.

2. Ventricular Pressure-Volume Relationships with Crossbridge Kinetics

Cardiac oxygen consumption is a reliable estimate of total energy expenditure of the heart, since it relies almost exclusively on oxidative metabolism, and is also an important indicator of its state of health. Although many famous researchers over the past century examined various parameters related to the performance of myocardial fibers (tension, length and shortening velocity), ventricular pressure, ventricular volume, and heart rate, those parameters failed to adequately predict cardiac oxygen consumption under varying loading conditions and contractile state[25]; reviewed by Suga[26]. In contrast, Suga demonstrated that oxygen consumption of the left ventricle is highly correlated to the mechanical energy utilized during a contraction, as determined from the left ventricular instantaneous pressure-volume (P-V) relation. This relation has become an important method for evaluating left ventricle performance at the chamber level, *in situ* and in cross-circulated hearts, in small and large animal models, as well as humans[25,27-36] and we believe will provide a wealth of information about macro function.

In brief, four phases during systole and diastole are clearly recognizable from each P-V loop that represents instantaneous changes in pressure and volume during a single cardiac cycle (Fig. 2). The first important finding from the reawakening of interest in pressure and volume analyses was an index of ventricular contractility (E_{max}), which is obtained from the slope of the end systolic P-V relation (ESPVR)[29]. Extensive use of E_{max} in the